



Review

Recent advances in electrochemiluminescence imaging analysis

Chengda Meng^{a,b}, Sara Knežević^c, Fangxin Du^{a,b}, Yiran Guan^{a,b}, Frédéric Kanoufi^d,
Neso Sojic^{c,*}, Guobao Xu^{a,b,*}



^a State Key Laboratory of Electroanalytical Chemistry, Changchun Institute of Applied Chemistry, Chinese Academy of Sciences, Changchun, Jilin 130022, China

^b University of Science and Technology of China, Hefei, Anhui 230026, China

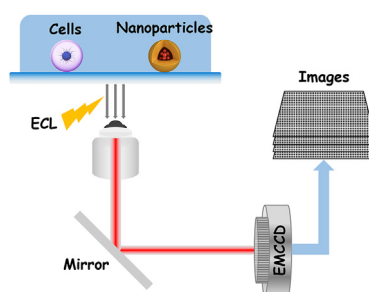
^c University of Bordeaux, Bordeaux INP, CNRS, UMR 5255, Site ENSCBP, 33607 Pessac, France

^d Université Paris Cité, ITODYS, CNRS, F-75013 Paris, France

HIGHLIGHTS

- Electrochemiluminescence technology and mechanisms are introduced.
- Various electrochemiluminescence imaging techniques are described.
- Progress in single-entity electrochemiluminescence imaging is reviewed.
- Advances in using electrochemiluminescence for fingerprint imaging are summarized.

GRAPHICAL ABSTRACT



ARTICLE INFO

Keywords:

Electrochemiluminescence
Imaging
Single-entity electrochemiluminescence
Single-molecule reaction
Single cell

ABSTRACT

Electrochemiluminescence (ECL) has been widely applied in imaging owing to features that distinguish it from other microscopic techniques and electrochemical methods, including its high signal-to-noise ratio, remarkable sensitivity, wide linear range, high spatiotemporal resolution, and near-zero background light. Imaging technology based on ECL has been used in the fields of immunosensing, pathological cell detection, and drug analysis. Additionally, its simple operation and ability to detect dynamic processes and catalytic sites strengthen its potential for research on material surfaces and interfaces, in vivo biological analysis, and cell visualization. At the same time, the emergence of a variety of nanomaterials and new microscopic analysis equipment has further promoted the development of high-resolution ECL imaging technology. This paper introduces the development of ECL technology and the mechanisms of the main ECL systems. It then describes various forms of ECL imaging methods, and reviews research progress on ECL imaging technology in the fields of single-particle imaging, fingerprint structure analysis, and single-cell microscopic imaging. Finally, the authors offer their views about the prospects for ECL imaging technology.

1. Introduction

Electrochemiluminescence (ECL) refers to the electrochemically triggered emission of light. In modern ECL, this arises from the redox reaction between a luminophore and a sacrificial co-reactant. The

emitted light is the analytically useful signal [1–11]. Detection based on this optical signal overcomes the problem of low sensitivity, enhancing it by several orders of magnitude. For example, the limit of detection (LOD) of $\text{Ru}(\text{bpy})_3^{2+}$ obtained by electrochemical methods is in the micromolar range, while with ECL it is closer to picomolar, and even single ECL

* Corresponding authors.

E-mail addresses: sojic@u-bordeaux.fr (N. Sojic), guobaouxu@ciac.ac.cn (G. Xu).

<https://doi.org/10.1016/j.esci.2022.10.004>

Received 29 July 2022; Received in revised form 17 September 2022; Accepted 26 October 2022

Available online 1 November 2022

2667-1417/© 2022 The Authors. Published by Elsevier B.V. on behalf of Nankai University. This is an open access article under the CC BY-NC-ND license (<http://creativecommons.org/licenses/by-nc-nd/4.0/>).

events may be measured with tripropylamine (TPA) as a co-reactant. This makes ECL a method of choice for bioassays [12–18]. Moreover, the technique's surface confinement, low background signal, and sensitive optical output, along with the dependence of its intensity on local electrode surface properties, make ECL a rising imaging/microscopy technique.

Various ECL imaging approaches have been developed by using conventional electrochemistry, bipolar electrochemistry, or wireless electrochemistry. Generally, we distinguish two main modes in ECL imaging: shadow ECL (SECL) and positive ECL (PECL). The two are closely related to the mechanistic routes by which ECL is generated, but their main difference is in the final images. While SECL creates a dark picture on a luminescent background, the PECL mode does the opposite, generating an image of a luminescent object on a dark background. PECL requires cell labeling, whereas SECL is a label-free method whereby the luminophore is dissolved in solution. Both modes have their advantages and are used accordingly in different studies. ECL imaging has been increasingly used in bioanalysis, cancer cell detection, cell surface biomolecular analysis, cell apoptosis monitoring, as well as the imaging of single cells, fingerprints, single particles (e.g., nanoelectrocatalysts), and single molecules. Given the developments in ECL-based methods over the last decade, various aspects of and trends in ECL and ECL microscopy have already been reviewed [19–29].

In this review, we introduce the principal features of ECL and the mechanisms of the main ECL systems, describe the various ECL imaging methods, summarize research progress in ECL imaging technology — from single-particle imaging and fingerprint structure analysis to single-cell and single-molecule microscopy — and comment on the prospects for ECL imaging technology.

2. ECL systems and mechanisms

In general, ECL involves two main processes: (i) excitation of a luminophore, consisting of an electrochemical and chemical (redox) step, and (ii) light emission (luminescence). The electrochemical reaction in

(i) generates the oxidized (and/or reduced) state of the luminophore and a highly unstable sacrificial co-reactant radical, which rapidly breaks down to form a strong reductant (or oxidant). The formed species react with each other by a very exergonic electron-transfer reaction and bring the luminophore into its excited state. A luminescence reaction (ii) occurs upon relaxation of the luminophore to its ground state. Depending on the experimental setup and the absence or presence of the co-reactant in the solution, we can distinguish two pathways: annihilation ECL and co-reactant ECL. As already mentioned, modern ECL technology relies mainly on the co-reactant pathway.

As typical ECL reagents, hydrazide compounds have the advantages of high luminescence efficiency, good reagent stability, low ECL potential in aqueous phase reactions, low cost, and low toxicity. Luminol is a standard example of this molecular family. In 1929, Harvey et al. reported the ECL properties of luminol for the first time, and the ECL mechanism and applications of related compounds have also been reported in a large number of studies since then. Its ECL mechanism is similar to that of CL. As shown in Fig. 1, the anion of luminol (LH^-) generates diazaquinone ($L^{\bullet-}$) through single electron transfer at the electrode, then is further oxidized by a superoxide radical ($O_2^{\bullet-}$) or hydrogen peroxide anion (HO_2^-) to a 3-amino-o-dicarboxylate anion ($AP_2^{\bullet-}$). After that, it returns to the ground state, accompanied by light radiation [30–36].

Another model ECL system is based on inorganic and metal–organic complexes. Studies have found that many metal clusters and redox polymers present ECL properties. For most transition metal compounds, the ECL is mainly derived from light emission upon the return of the energy excited state to the ground state, because the coupling of the spin orbit results in rapid spin-allowed excited state inactivation. In many cases, these excited states can only exist for a very short time, and phosphorescence is generated mainly through spin-blocking in the excited states. Numerous complexes of various metals, such as ruthenium, osmium, chromium, cadmium, palladium, platinum, rhenium, iridium, molybdenum, terbium, europium, and copper, have shown ECL. $Ru(bpy)_3^{2+}$ has been studied extensively due to its excellent photo-

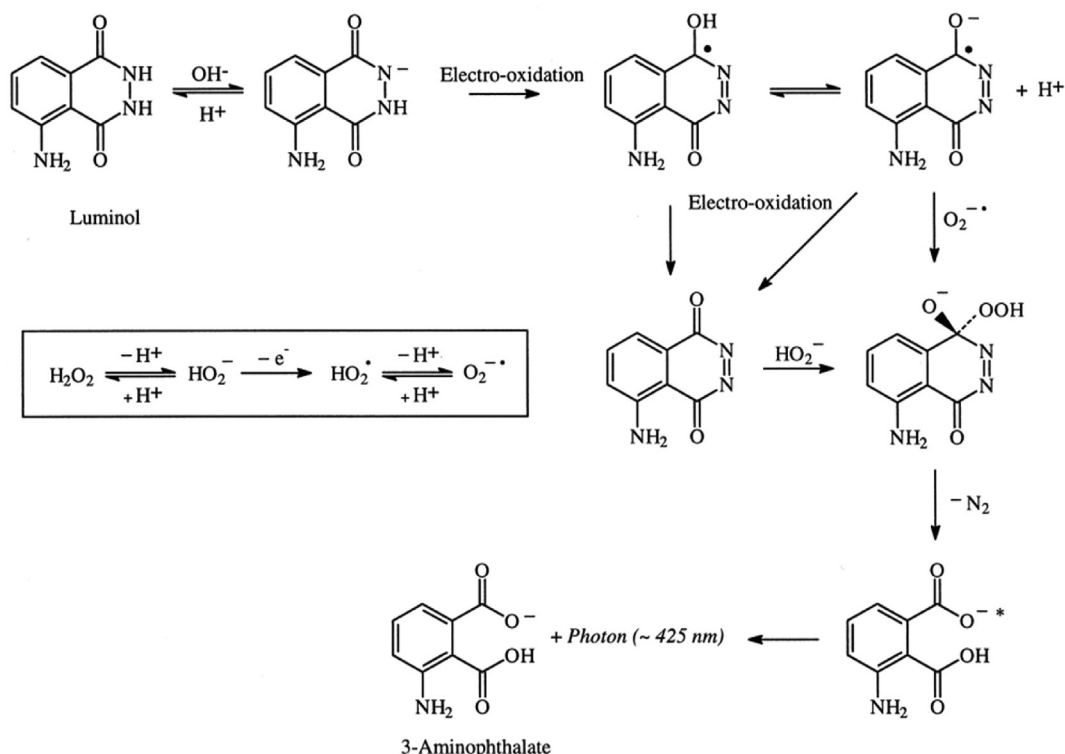
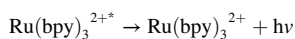
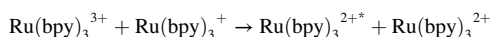
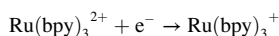
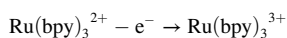


Fig. 1. Proposed mechanism for the ECL reaction of luminol [36]. Reproduced from Ref. [36] with permission from Elsevier.

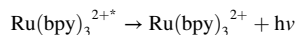
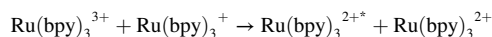
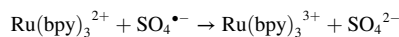
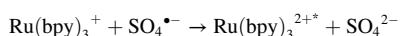
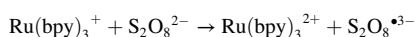
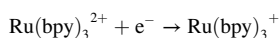
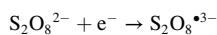
physical and electrochemical properties. It plays an important role in theoretical research and analytical/imaging applications of ECL. In this system, ECL shows the following characteristics: (a) the analysis can be carried out in neutral aqueous solutions or organic solutions. (b) It is insensitive to the presence of impurities and dissolved dioxygen. (c) Stable ECL can be produced at room temperature and at relatively low anodic potentials. (d) The luminophore is regenerated during the ECL process, and it can be “reused” (returned to the ground state without decomposition or other chemical changes), unlike the co-reactant species [37,38].

In 1972, Bard's group observed annihilation ECL by applying positive and negative potentials to Pt electrodes in acetonitrile containing $\text{Ru}(\text{bpy})_3^{2+}$. When the working electrode is rapidly pulsed between sufficiently positive and negative voltages to generate $\text{Ru}(\text{bpy})_3^+$ and $\text{Ru}(\text{bpy})_3^{3+}$ from $\text{Ru}(\text{bpy})_3^{2+}$, the two can react to form the excited $\text{Ru}(\text{bpy})_3^{2+*}$. ECL is generated by the transition of the excited state back to the ground state, causing the emission of red light at 620 nm; this can be described by the following reactions [39–41].



$\text{Ru}(\text{bpy})_3^{2+}/\text{TPA}$ is the most studied co-reactant ECL system at present, and several competitive ECL reaction routes have been proposed. After the application of unidirectional anodic potential, $\text{Ru}(\text{bpy})_3^{2+}$ and TPA are oxidized to $\text{Ru}(\text{bpy})_3^{3+}$ and TPA^+ , respectively. The cation radical then loses a proton to produce a strong neutral reductant, TPA^\bullet . As shown in Scheme 1a, the redox reaction between $\text{Ru}(\text{bpy})_3^{3+}$ and TPA^\bullet is highly exergonic and results in the formation of the excited state, $\text{Ru}(\text{bpy})_3^{2+*}$. Scheme 1b shows that TPA^\bullet can also reduce $\text{Ru}(\text{bpy})_3^{2+}$ to produce $\text{Ru}(\text{bpy})_3^+$, which then reacts with electrogenerated $\text{Ru}(\text{bpy})_3^{3+}$ to generate ECL. Scheme 1c shows the “catalytic” route involving homogeneous oxidation of TPA with $\text{Ru}(\text{bpy})_3^{3+}$ [42]. The heterogeneous or remote route (Scheme 1d) involves direct oxidation of TPA on the electrode surface, yielding $\text{TPA}^{\bullet+}$ and, by its deprotonation, TPA^\bullet . TPA^\bullet reduces $\text{Ru}(\text{bpy})_3^{2+}$ to $\text{Ru}(\text{bpy})_3^+$, which is subsequently oxidized to $\text{Ru}(\text{bpy})_3^{2+*}$ by $\text{TPA}^{\bullet+}$. This route is only possible when using the luminophore as a label, immobilized on a non-conductive object, and its surface confinement is due to the short lifetime of $\text{TPA}^{\bullet+}$ [43]. Recently, Zanut et al. have proposed an additional short-distance reaction route involving a N-centered dipropylamine radical generated by C–N bond cleavage in concert with TPA oxidation (Scheme 1e) [44].

$\text{Ru}(\text{bpy})_3^{2+}/\text{persulfate}$ ($\text{S}_2\text{O}_8^{2-}$) is a typical reduction–oxidation cathodic ECL system. First, both are reduced to form $\text{Ru}(\text{bpy})_3^+$ and $\text{SO}_4^{\bullet-}$, and their reaction results in the formation of the $\text{Ru}(\text{bpy})_3^{2+*}$ excited state, followed by light emission [45,46]:



At present, ECL of $\text{Ru}(\text{bpy})_3^{2+}$ with $\text{S}_2\text{O}_8^{2-}$ is rarely used in aqueous solutions because it requires negative reduction potentials and has hydrogen evolution as a side reaction.

3. ECL imaging analysis

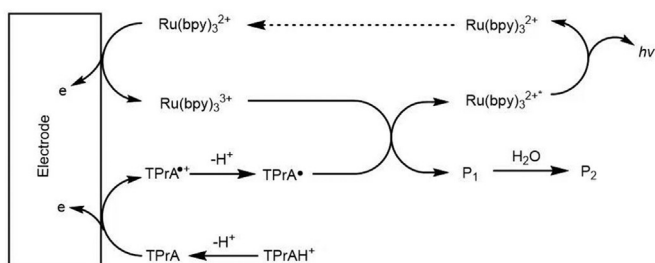
3.1. ECL imaging

Currently, the common ECL sensing technology mainly uses a photomultiplier tube (PMT) and other photodetectors to collect the photons generated by the whole surface of an electrode, then outputs the corresponding ECL signal after amplification. PMT-based ECL devices have been widely used in many fields of analytical chemistry, especially in medical research and biological analysis, due to its simple structure and low cost. PMT-based ECL detection can also be arranged to record the luminescence intensity over a localized region of an electrode. This is the principle of confocal microscopic ECL imaging: a pinhole aperture is used to collect the photons emitted only from a focused diffraction-limited spot of a sample, here a region of an electrode. Scanning the focused spot over the sample allows imaging of its ECL distribution. Confocal microscopy has been used to resolve spatially (then image) ECL distribution at microelectrodes [47,48].

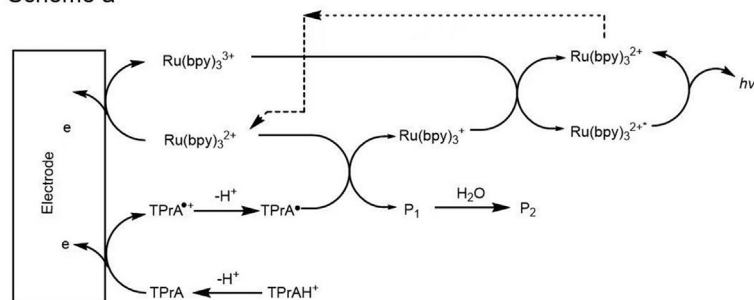
Similarly, but without scanning the photon detector, a CCD (charge coupled device) camera allows photons to be collected instantaneously by a large array of detectors (e.g., 1024×1024 detectors for a 1 M pixel camera). This offers another way of collecting ECL imaging and outputting an ECL signal in the form of an image, without having to scan samples with the detector. The main components of such ECL imaging setups include a potentiostat and a bright field microscope (or objective microscope) equipped with a CCD or EMCCD (electron multiplier CCD) camera. By selecting the appropriate electrochemical conditions and techniques, electrode structure, and solution composition, the thickness of the ECL active region and the lateral resolution of the ECL imaging techniques are tunable. Typically, the thickness of the ECL reaction layer is in the micrometer range. It can be decreased with higher concentrations of co-reactant. The lateral resolution is usually similar to that in classic optical microscopy techniques. This type of ECL imaging technology, developed in recent years, can provide optical images and electrochemical signals at the same time, and can meet the analytical science requirements for high throughput, visualization, and information diversification. ECL imaging systems play an important role in both macro and micro analysis [49–53].

3.2. ECL imaging based on BPE

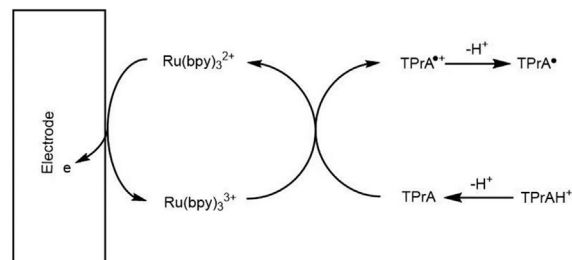
A bipolar electrode (BPE) is a conductive object placed between an anode and a cathode (named the feeder electrodes) in an electrolytic cell containing a given electrolyte [54]. The conductor is not directly connected with the power supply, whereas the feeder electrodes are. But when a voltage is imposed between the two feeder electrodes, the applied electric field induces a potential difference between the two ends of the conductor, one becoming polarized into a cathode and the other into an anode. Due to the potential difference between the two ends of the bipolar electrode and the solution, oxidation and reduction reactions occur simultaneously at both ends of the bipolar object. When a sufficient voltage is applied between the feeder electrodes, a reduction reaction takes place at the cathodic end of the BPE, and the ECL of a $\text{Ru}(\text{bpy})_3^{2+}/\text{TPA}$ or luminol/ H_2O_2 system is localized (and imaged) at its



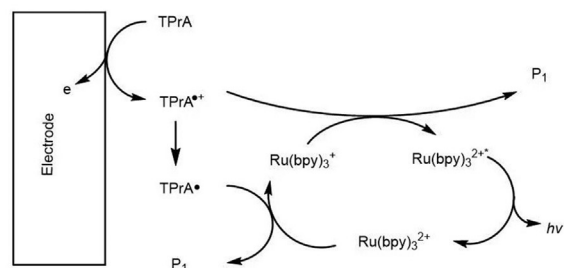
Scheme a



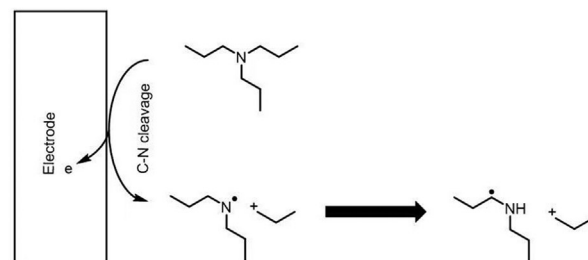
Scheme b



Scheme c



Scheme d



Scheme e

Scheme 1. ECL reaction routes of $\text{Ru}(\text{bpy})_3^{2+}/\text{TPA}$ ECL [42–44]. Reproduced from Refs. [42–44] with permission from the American Chemical Society and Nature Portfolio, respectively.

anodic end. The ECL image is collected by a CCD camera and transmitted to a computer for image information analysis [55–59]. A mobile phone has also been reported to image multicolor ECL emission [54].

Cao et al. developed a BPE ECL imaging strategy based on closed bipolar electrodes (Fig. 2) [2]. They used a functional nanoprobe of heterogeneous $\text{Ru}(\text{bpy})_3^{2+}/\text{SiO}_2/\text{Au}$ nanoparticles for a visual immunoassay of prostate-specific antigen (PSA) on a single cell. Based on the synergistic amplification effect of anode and cathode amplification, a multiple auxiliary ECL signal amplification strategy was introduced into the detection system. This was also used to evaluate the level of PSA in serum samples. The sensing platform could not only detect tumor markers in body fluid but also measure their expression in a single cell.

Douman et al. constructed a radio chemiluminescence system using interdigitated, 3D-printed titanium arrays as feeder electrodes. The micro-emission was gold microparticles (45 μm diameter) functionalized with 11-mercaptoundecanoic acid. A $\text{Ru}(\text{bpy})_3^{2+}/\text{TPA}$ system was used to produce ECL. Depending on the geometry of the electrode array, the oxide-coated titanium eliminated the need to add an electrolyte to the process that generated the electric field. They mapped the distribution of electric fields using COMSOL simulations and ECL imaging with long exposures. At the same time, the surface charge of the gold particles could be controlled by pH and the ECL intensity was thereby affected [60].

3.3. ECL imaging based on wireless transmission

A BPE provides a way to achieve ECL without a direct connection to the electrode. Although some reports call it a “wireless” technology, electron transfer still requires a conductive material or feeder electrodes in a solution as the carrier, rather than this being truly wireless transmission. What is often called wireless transmission technology refers to there being a space separating the power generation device and the electric device; these are not directly connect by wires, so the electric energy is transmitted by electromagnetic induction and other ways. Xu et al. designed a wireless ECL device by using wireless transmission technology, as shown in Fig. 3 [61]. The transmitter end of the radio is a wireless transmitting coil, the receiver end is a copper coil, and the two ends of the copper wire are connected to the working electrode and the opposite electrode, respectively. ECL detection of H_2O_2 can be performed with luminol without any direct electrical contact between the electrochemical driving device and the electrode.

J. Totoricaguena-Gorri proposed a device based on a rectified antenna and a double-electrode electrochemical battery, both of which were printed on a thin plastic substrate. A rectifier antenna is a rectifier device composed of an antenna coupled to a rectifier circuit. Rectifier antennas convert an alternating current (AC) signal to a direct current (DC) voltage, and they are mainly used for radio frequency (RF) to DC power conversion. The rectifier antenna can use near-field communi-

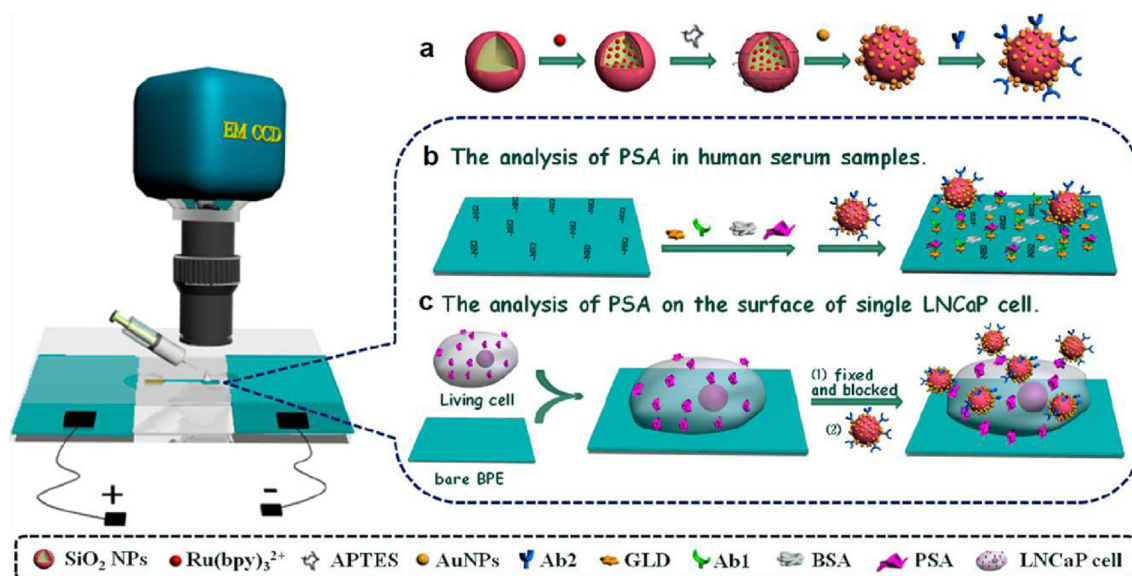


Fig. 2. Construction of the ECL assay interface on the anodic pole of the BPE, and schematic setup used for ECL imaging [2]. Reproduced from Ref. [2] with permission from the American Chemical Society.

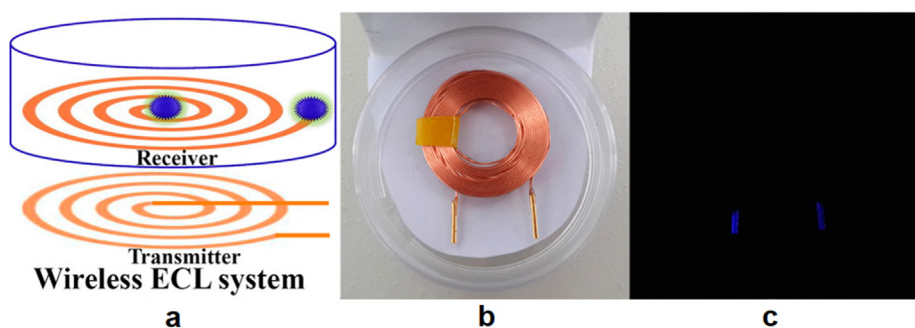


Fig. 3. Schematic representation of the wireless ECL system (a), photo (b) and ECL image (c) of the wireless ECL mini-device using two short gold wires with small, lacquered copper coils [61]. Reproduced from Ref. [61] with permission from the American Chemical Society.

cation (NFC, 13.56 MHz) signals to provide the energy needed to generate ECL from $\text{Ru}(\text{bpy})_3^{2+}/\text{TPA}$. The intensity of the light emitted is proportional to the concentration of the ruthenium complex and can then be captured and analyzed by a mobile phone camera. The method and device are easy to use and constitute the first application of NFC in an ECL system [62].

3.4. ECL imaging based on multi-electrode array

ECL has also impacted the interdisciplinary research field of analytical chemistry for life sciences, where the focus is on the detection of the numerous chemical components involved in biological activities, as well as the exploration of new detection principles and analysis methods. Electrochemical analysis, especially ECL, is a common detection method that has been combined with biochip technology, and many ECL biochips have been developed by researchers. Among these, electrode arrays have many advantages, such as integration, miniaturization, and general quantization [61,63–66]. ECL imaging with microarray electrodes can also reduce the number of samples required to be examined and provide a high spatial resolution analysis method.

Wireless ECL is a particularly interesting strategy for implementation in the multiple instruments used for analysis in the life sciences (microscopes, cell culture chips, etc.). However, the wireless energy transmission module induces an alternating potential waveform at the receiver electrode, resulting in the electro-generation of different active intermediates that interfere with and weaken the ECL generation. Xu's team proposed a strategy to circumvent this issue using a wireless ECL electrode array chip [67]. As shown in Fig. 4, by implanting a rectifying diode in the receiver branch of a circuit, a stable direct potential/current is obtained, thus increasing the ECL efficiency and luminescence intensity by 18,000 times. The introduction of a diode is more conducive to visual detection with a luminol/ H_2O_2 system, and it also reduces the performance requirements of the image acquisition equipment (camera), lowering the equipment cost. In addition, the array chip can be used for simultaneous detection of multiple concentrations or components, which greatly improves analytical efficiency.

The preparation of BPE arrays is technically demanding. Iwama et al. proposed a new manufacturing scheme for the large-scale production of

an array comprising bundles of carbon fiber-based BPE (cBPE) with high precision and yield [68]. Their approach was based on a highly reproducible thermal stretching process, optimized for fabricating a single-electrode fiber from a carbon nanofiber composite. After demonstrating the fiber's applicability in a cBPE-ECL system, they prepared a multi-electrode fiber (each with a diameter in the range of tens of micrometers) by the thermal stretching of 104 single-electrode fibers. The feasibility of using this multi-electrode fiber as a cBPE array for ECL imaging was confirmed, and the functional rate was 99%. They also discussed miniaturizing the cBPE and therefore the ECL imaging resolution. This relies on miniaturizing the carbon micro/nanofibers in conjunction with thinning the fiber bundle using the principle of thermal stretching.

Sentic et al. fabricated a nanodisk array electrode and nanoribbon array electrode with different spacing sizes using electron beam lithography of a polycarbonate layer on boron-doped diamond (BDD) [69]. In addition, 16 different geometric shapes were etched on the same BDD substrate to form a multiple nanoelectrode and ultramicroelectrode array platform (MNEAP). Imaging experiments using a $\text{Ru}(\text{bpy})_3^{2+}/\text{TPA}$ system (Fig. 5) simultaneously showed the effects that modulating the dimensions and shapes of the electrode arrays had on the imaging resolution and sensitivity. In high concentrations of TPA, point-like or banded ECL imaging with good separation (high resolution) was obtained, and the thickness of the ECL spot or band was correlated with the TPA concentration. However, the ECL image produced with nano-electrodes arrays in which the size and spacing of the nano-electrodes were small was diffraction limited: the thickness of an individual band or spot was difficult to distinguish (resolve) clearly, which limited its application for imaging. The nanoelectrode arrays did produce much higher ECL signals, making them of interest for more sensitive detection devices.

Disposable flow ECL-based assays have been considered by Wang et al., who designed a potential-resolved paper-based biosensor based on a BPE array. They used wax printing technology, screen printing technology, and gold nanoparticles (AuNPs) grown in situ to prepare a paper-based microfluidic sensing platform with a hydrophilic zone, hydrophobic boundary, waterproof electron bridge, driving electrode region, and parallel bipolar electrode region. CdTe quantum dots (QDs)- H_2 and Au@g- C_3N_4 nanosheets (NSs)-DNA1 were used as dual ECL signal probes, and carboxylated Fe_3O_4 magnetic nanoparticles functioned as carriers. The detection of two kinds of RNA (miRNA-155 and miRNA-126) was realized. The combination of this bipolar electrochemical system and potential-resolved multitarget ECL could reduce spatial interference and provide an effective method for clinical application [60].

In addition to conventional three-electrode systems and bipolar electrochemical systems using electrode arrays, single-electrode electrochemical systems (SEES) have also attracted substantial attention. Compared to multi-electrode array electrochemical systems, the SEES is characterized by its simplicity, cost-effectiveness, and user-friendliness. At the same time, the detector is flexible and has great development potential. Du et al. developed a SEES for visual high-throughput ECL immunoassay. Based on the resistance sensing potential difference, the system attaches plastic stickers with multiple holes to a single carbon ink screen printing electrode, thus forming an intuitive and simple detection device. Because of the efficient adsorption and biological affinity of the carbon inks, antibodies can be immobilized on inkjet-printed carbon mesh electrodes. The cardiac troponin I (cTnI) marker can be captured by cTnI antibody immobilized on an electrode surface. When the electrode triggers the ECL of the luminol- H_2O_2 system, marker recognition results in a decrease in the ECL intensity. The assembly and labeling process could be simplified using a smartphone as a detector. The ECL composite immunoassay developed based on this device is simple and rapid, which is of great significance for the accurate and rapid detection of cTnI and for the early diagnosis and treatment of acute myocardial infarction [70].

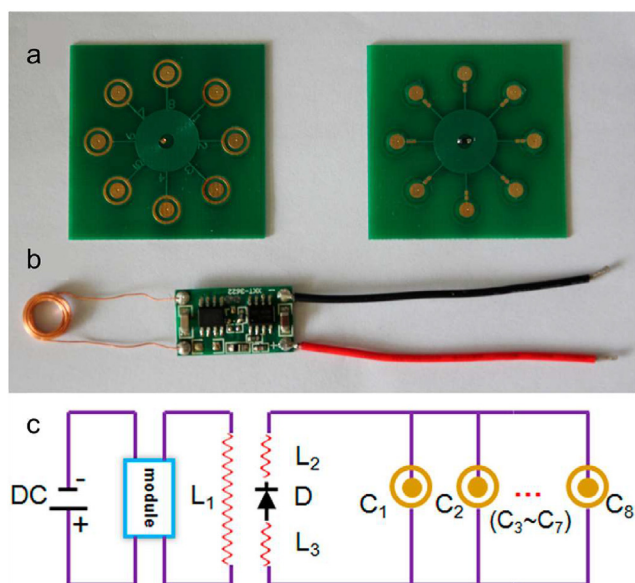


Fig. 4. Schematic representation of the wireless ECL detection mini-device (a, b) and its working circuit (c), showing the use of a rectifying diode to suppress the alternating current waveform in the reception branch [67]. Reproduced from Ref. [67] with permission from the American Chemical Society.

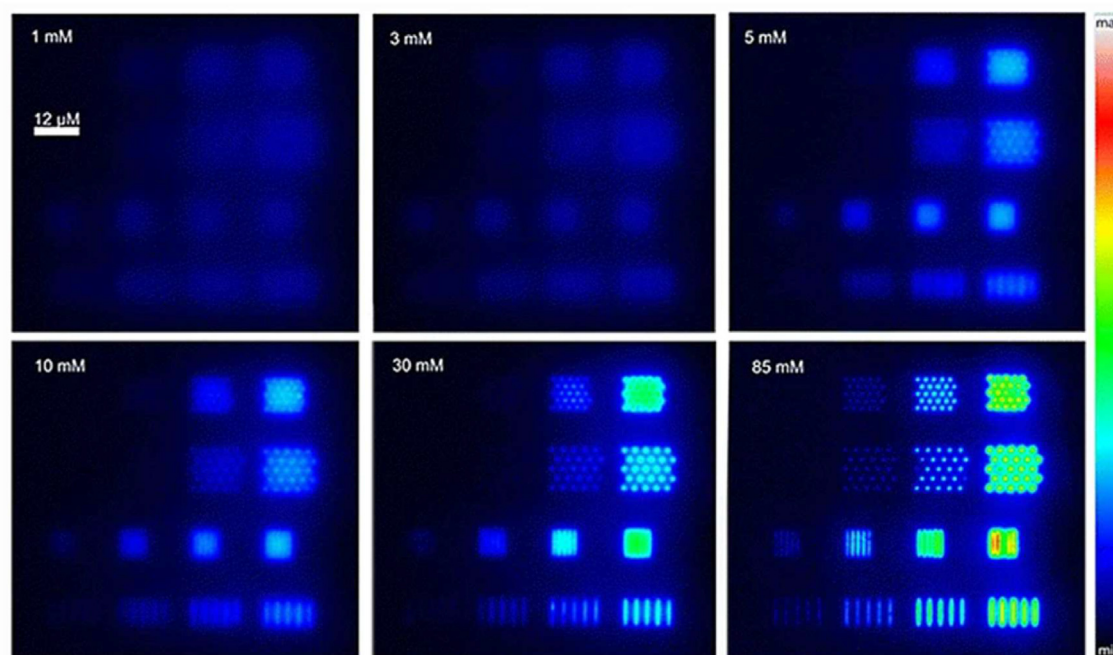


Fig. 5. ECL images of the MNEAP obtained in a PBS solution (pH 7.4) containing both 1 mM $\text{Ru}(\text{bpy})_3^{2+}$ and increasing concentrations of TPA (indicated in the top-left corner of each box) [69]. Reproduced from Ref. [69] with permission from Springer Nature.

4. Application of ECL imaging analysis

4.1. ECL imaging of single particles

The last two decades have witnessed increased interest in the evaluation of electrochemical activity at the single entity level. This is of particular importance when dealing with nanoparticles. Indeed, within an ensemble of nanoparticles, in solution or assembled on an electrode surface, one may probe a population that contains a large range of sizes, geometries, surface chemistries, etc. This results in wide variability of the intrinsic electrochemical activity, which is often undetected in macro-scale electrochemical measurement that averages across a given population. The heterogeneity of single-particle activity, and ultimately the intrinsic activity of a single particle, can only be revealed by probing particles one by one, at the single entity level [71]. This is generally achieved by diluting the particle sample in either time or space. Dilution in time means detecting on a sensor one particle at a time. In electrochemistry, it corresponds to the nano-impact electrochemistry approach, which consists of probing the stochastic collision of individual particles on a miniaturized electrode [72]. Dilution in space consists of confining one nanoparticle on a tiny electrode region and imaging its electrochemical activity with a high-resolution microscope. Different microscopies and confinement strategies, using scanning electrochemical probes such as nanoelectrodes and nanopipettes [73], have been proposed, among which super-localization optical microscopes are interesting candidates [74,75]. Of the latter, ECL microscopic imaging has become a useful tool for imaging and measuring single particles.

Bard et al. pioneered the observation of single-particle collisions using ECL [76,77]. The collision of single platinum nanoparticles with an indium tin oxide electrode enhances the ECL strength. In a catalytic solution containing $\text{Ru}(\text{bpy})_3^{2+}$ and TPA (or other auxiliary reactions), each collision produces a unique photon peak related to the size and concentration of platinum nanoparticles. By adjusting the type of measuring electrode and reaction system, controllable ECL intensity amplification can be obtained [76]. Based on the research results of Bard et al., Pan et al. proposed a mechanism using gold nanoparticles to enhance the oxidation of TPA and the ECL intensity of $\text{Ru}(\text{bpy})_3^{2+}$; they reached a

similar conclusion that ECL intensity increases with particle size and is affected by the nanoparticles' local chemistry and charge transfer environment. On this basis, a new method has been developed to study the local redox activities of large Au particles, Au nanoparticles, and Au nanowires [78].

Ma et al. developed ECL microscopic imaging technology using a nanoscale single particle (Fig. 6) to analyze local electrochemical reactions [25]. They measured the ECL of nanoparticles on the surface of a glassy carbon electrode (GCE) using a water immersion microscope objective lens with a high numerical aperture. This imaging technique has high temporal and spatial resolution and light collection efficiency, and it can simultaneously monitor the transient collisions of multiple nanoparticles. Of particular interest is the ability to detect particles within the solution ca. 200 μm above the electrode, providing a 3D dynamic trajectory of a particle. Observing such a trajectory before and after the particle impacts the electrode complements the kinetic information derived from collision electrochemistry [79,80]. ECL imaging results show that the collision type, collision frequency, and luminescence intensity of a single particle are significantly correlated with the electrode surface properties (electrode edges effects) and the particle concentration. Based on continuous collision events, they designed a "relay detection" method to monitor changes in analyte concentration in real time, providing a way to observe collision behavior at the single particle level and achieve visual detection.

Sojic et al. imaged liposomes using an ECL method and realized the quantitative detection of liposome release. They encapsulated $\text{Ru}(\text{bpy})_3^{2+}$ /TPA in sealed liposomes made of DOPC/DOPC phospholipids. After their sedimentation on an ITO electrode, the opening of the liposomes was then triggered by polarization of the ITO, and the release of their contents induced ECL emission. The imaging detection of liposomes was realized by a combination of the amperometric method, fluorescence imaging, and ECL imaging. ECL mainly provided imaging of substance outflow after the liposomes opened [81].

Nanoparticles are widely used in heterogeneous catalysis because of their large specific surface area and high density of active sites. Due to the different distribution patterns of atoms on the point, line, and surface of a single particle, each particle has a different size and shape.

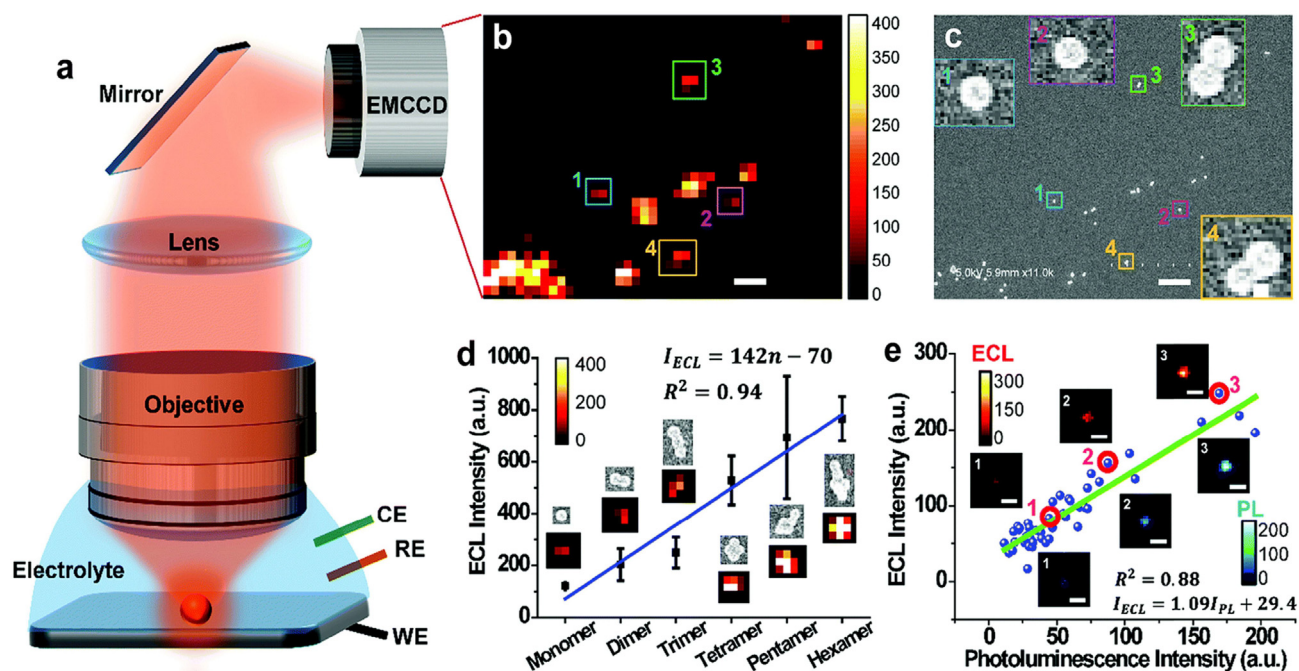


Fig. 6. Schematic illustration of the ECL microscopy setup for single particle ECL imaging and the relationship between particle size and intensity [25]. Reproduced from Ref. [25] with permission from The Royal Society of Chemistry.

These differences in surface structure mean each single particle has a different catalytic effect. Some noble metal nanoparticles have high catalytic capacity in electrochemical reactions. Therefore, the analysis of the relationship between particle structure and catalytic performance at the single particle level is of great help for optimizing synthesis methods and improving particles' intrinsic catalytic activity. With its high spatial resolution, ECL microscopic imaging can collect imaging information about different particles at the same time and intuitively reflect differences between single particles' catalytic capacity. Zhu et al. prepared double-faced (Janus) gold–platinum particles (Au–Pt JNPs), as shown in Fig. 7 [16]. They observed Au NPs, Pt NPs, and Au–Pt JNPs with an ECL microscope and found that Au–Pt JNPs showed higher ECL

catalytic activity compared with single metal NPs. These differences were explained, based on numerical simulations, by the higher electron transfer rate at the Pt surface of the JNP than at the Au surface. This asymmetric catalysis of the luminophore resulted in an asymmetric concentration gradient around the particles, which induced fluid flow around each particle and therefore enhanced mass transfer (higher ECL activity), as well as reduced competing reactions such as oxide layer formation (because of lower particle surface passivation or higher ECL stability). This experiment provides a new method to study the electrochemical and electrocatalytic activity of single nanoparticles using ECL imaging at high throughput but without an external light source [82,83].

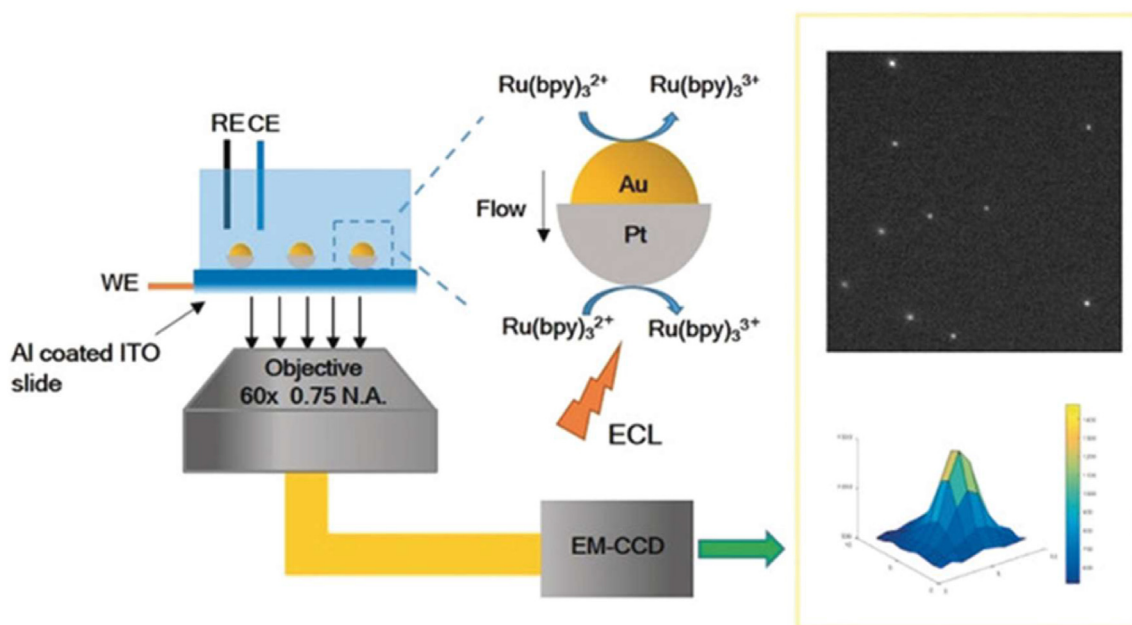


Fig. 7. ECL imaging of electrocatalysis at a single Au–Pt JNP [16]. Reproduced from Ref. [16] with permission from John Wiley and Sons.

The size, shape and catalytic activity of nanocrystals can be imaged at the submicron level based on ECL microscopy. In addition, the relationship between the structure, surface properties, and electrochemical activity of nanoparticles can be analyzed with an ECL microscope. Xu et al. studied the electrocatalytic activity of different regions of a single 2D gold nanoplate. Through finite element simulation, the distribution of ECL on the micron plate was determined to be relatively uniform. The non-uniform distribution in a single nano-plate was due to the time-dependent spatial distribution of electrocatalytic activity on different surfaces; the corners and edges, which had more defects, had high catalytic activity, but their catalytic stability was lower than that of the plane [32]. Zhu et al. reported the electrocatalytic performance of zinc oxide crystals. They synthesized ZnO crystals ($> 20 \mu\text{m}$ long) with various proportions of exposed facet. Through visual analysis using an ECL microscope at the submicron level, they found that the crystal face of zinc oxide (002) had better catalytic performance than the mirror surface of (100). The visualization of spatial heterogeneity in electrocatalytic activity on different sides of the same particle was realized with micrometer-level resolution [84].

Nanoscale spatial resolution imaging is afforded by using the concepts of super-localization, commonly employed in super-resolution optical microscopies. Briefly, it consists of localizing with the highest precision possible an optical event within an optical image. It can be obtained by estimating the position (also named center of mass) of the diffraction limited pattern corresponding to the nanoparticle image — for example, by a 2D Gaussian fit of the optical intensity profile. This position is usually obtained with 5 nm localization precision. Such a strategy usually requires that the nanosized object be imaged using a microscope objective lens with a high numerical aperture to have sufficient pixels over the diffraction limited pattern (typically > 3 pixels over 500 nm). This condition is technically demanding, as it requires a much higher number of emitted photons, which may be an issue under ECL conditions. Ultra-sensitive cameras are now capable of reaching the ultimate detection of single photons. ECL is a perfect playground for such cameras, since it allows the generation of photons without an external source of light and therefore a near-zero optical signal background. This was recently demonstrated by Feng's group within a $\text{Ru}(\text{bpy})_3^{2+}/\text{TPA}$ ECL system [85,86]. In highly diluted solutions, it is possible to engage an ECL reaction with a single luminophore molecule. The reaction is triggered by the electrochemical oxidation of TPA at an electrode. This ensures a further dilution of the reactive intermediate radical species near the electrode surface, enabling a single excited state production (and luminescence) event [87]. Ideally, this single luminescence event is detected as a single pixel in an image acquired by short (millisecond) exposure. By acquiring and overlaying successive short-exposure images of the electrode surface, one can reveal regions of different ECL activity, thereby achieving single-molecule sensitivity. This single-molecule ECL microscopy provides a super-resolution (sub-micrometer) mapping of electrodes or catalytic activity, and it has been used to image local electrocatalytic activity within a $1 \mu\text{m}$ Au hexagonal plate with a 37 nm spatial resolution. Within these nanometer domains, it is further possible to track the turnover frequency of the electrocatalytic activity of Au for $\text{Ru}(\text{bpy})_3^{2+}$ oxidation with its applied potential.

Aside from analyzing the species involved in the electrocatalytic reactions scheme producing the ECL, different co-reactant electrocatalytic reactions can be analyzed using ECL microscopies. The luminol system is of particular interest, as it involves the oxygen reduction reaction (ORR). Observing and quantifying the amount of ECL generated with the luminol system at different electrodes then allows one to inspect the electrocatalytic activity of these different electrode materials for the ORR. A strategy was recently proposed by Xia et al. to inspect the formation of reactive oxygen species involved in the ORR. It was possible to discriminate between the formation of $\text{O}_2^{\bullet-}$ via a 2-electron reduction path or its combination with HO^\bullet via a 4-electron path. The strategy was used to show that the ORR activity of single Fe atom catalysts was mostly

driven by the 4-electron path [88]. Combined with ECL imaging, this strategy should be promising for screening the ORR activity of catalysts.

Based on a single-molecule positioning microscope (SMLM), Chen et al. achieved the capture of a single photon in an ECL reaction and designed super-resolved electrogenerated chemiluminescence microscopy (ECLM) for ECL imaging [89]. Based on ECLM, they realized real-time imaging of the surface-related catalytic activity of nanocatalysts. The super-resolved ECLM they used can measure the activity of specific faces or positions of individual nanoparticles in the range of nanometer resolution. The spatial resolution of the ECL image obtained by them was up to 100 nm, revealing more details of the electrocatalytic reaction. In addition, they also determined the catalytic activity distribution on Au nanorods or nanoplates at the hundreds of nanometers level using super-resolution ECLM. This is of great significance for revealing the surface activity at surfaces or defects and can reflect the dynamic fluctuation of single nanoparticles.

Overall, these recent strategies combining high-resolution ECL imaging and nanoelectrocatalysts considerably widen the possibilities of using ECL imaging to achieve a more comprehensive exploration of the reaction modes of nanocatalysts.

4.2. ECL imaging of fingerprints

Fingerprints are impressions left by the touch of a fingertip on a surface. They play an important role in forensic investigations, personal identification, security checks, and access control. However, latent fingerprints (LFP) are usually difficult to identify directly with the naked eye or instruments. Traditional LFP developing techniques include powder developing, smoke developing, ninhydrin developing, and UV testing. Because of the toxicity of the necessary reagents and dyes, long-term exposure can affect technicians' health. The brushing and dyeing processes can also cause permanent damage to valuable evidence.

Su's group [90] applied ECL imaging technology to LFP analysis for the first time, obtaining two ECL imaging modes: inverse or reverse phase and positive or forward phase. In the inverse mode, the ECL reaction can only take place in regions not covered by fingerprints, because some inert components (such as fatty acids) in fingerprints can hinder electron transfer. In the forward mode, some ECL imaging information can be obtained on the fingerprint because the luminescent molecules are labeled on it. Later, Su's group applied LFP ECL imaging technology to the detection of certain metabolites in fingerprints [91]. Biotin-labeled antibodies bind to the antigens in a fingerprint through immune recognition. By using the specific recognition of biotin and streptavidin, streptavidin-functionalized horseradish catalase (HRP) was attached to a fingerprint. HRP catalyzed the decomposition of H_2O_2 , and a luminol/ H_2O_2 system ECL was realized in the fingerprint region, so the relevant information for determining the fingerprint structure was obtained. They also polymerized luminol on the ITO electrode to cover the fingerprints deposited on the electrode surface, forming a negative ECL image [92].

4.3. ECL imaging of cells

The development of ECL imaging introduced a new dimension to single-cell analysis due to its time- and space-resolved properties, very low background signal compared to photoluminescence (PL), and high selectivity, specificity, and sensitivity. However, non-invasive detection of intracellular compounds remains a challenge. Different approaches suggest using specifically designed materials [93], microwells [94], and even wireless bipolar nanodevices [95] to selectively detect analytes in a single cell. Furthermore, as mentioned in the previous section, single entity imaging has been developed during the past decade for microbeads, magnetic nanoparticles, and bipolar electrodes, but that technology has not been adopted for the imaging of cells.

Recently, single cells were imaged using an ECL-based microscopy approach with a model $\text{Ru}(\text{bpy})_3^{2+}/\text{TPA}$ system [96]. CHO cells were grown on a glassy carbon electrode surface and subsequently biotinylated to enable binding of the streptavidin–ruthenium label to the cell membrane. Images of the labeled cells showed that the ECL signal was located on cell borders, suggesting that the membrane was impermeable to co-reactant species. Indeed, the freely diffusing TPA co-reactant reacted only at the bare electrode surface in the vicinity of the cells. This important limitation upon the further development and potential applications of the ECL method was overcome by making the cell membrane permeable with Triton X, allowing the TPA to diffuse through and reach the electrode surface, where it was oxidized [97]. Compared to

PL, ECL allows the visualization of a larger area of the cell contour, which can be ascribed to its better signal-to-background ratio. Additionally, the focal plane of ECL is closer to the electrode surface due to the surface-confined nature of ECL, conditioned by the short lifetimes of electrogenerated TPA^{\bullet} and $\text{TPA}^{+\bullet}$ radicals that produce the excited state of the luminophore in the heterogeneous co-reactant mechanism. Since only the basal membrane generates ECL, this technique can image details that are very difficult to discern using fluorescence microscopy. The method can be further modified to suit diagnostic applications by utilizing transparent and disposable inkjet-printed carbon nanotube electrodes, which also allows for ECL imaging in both transmission and reflection mode.

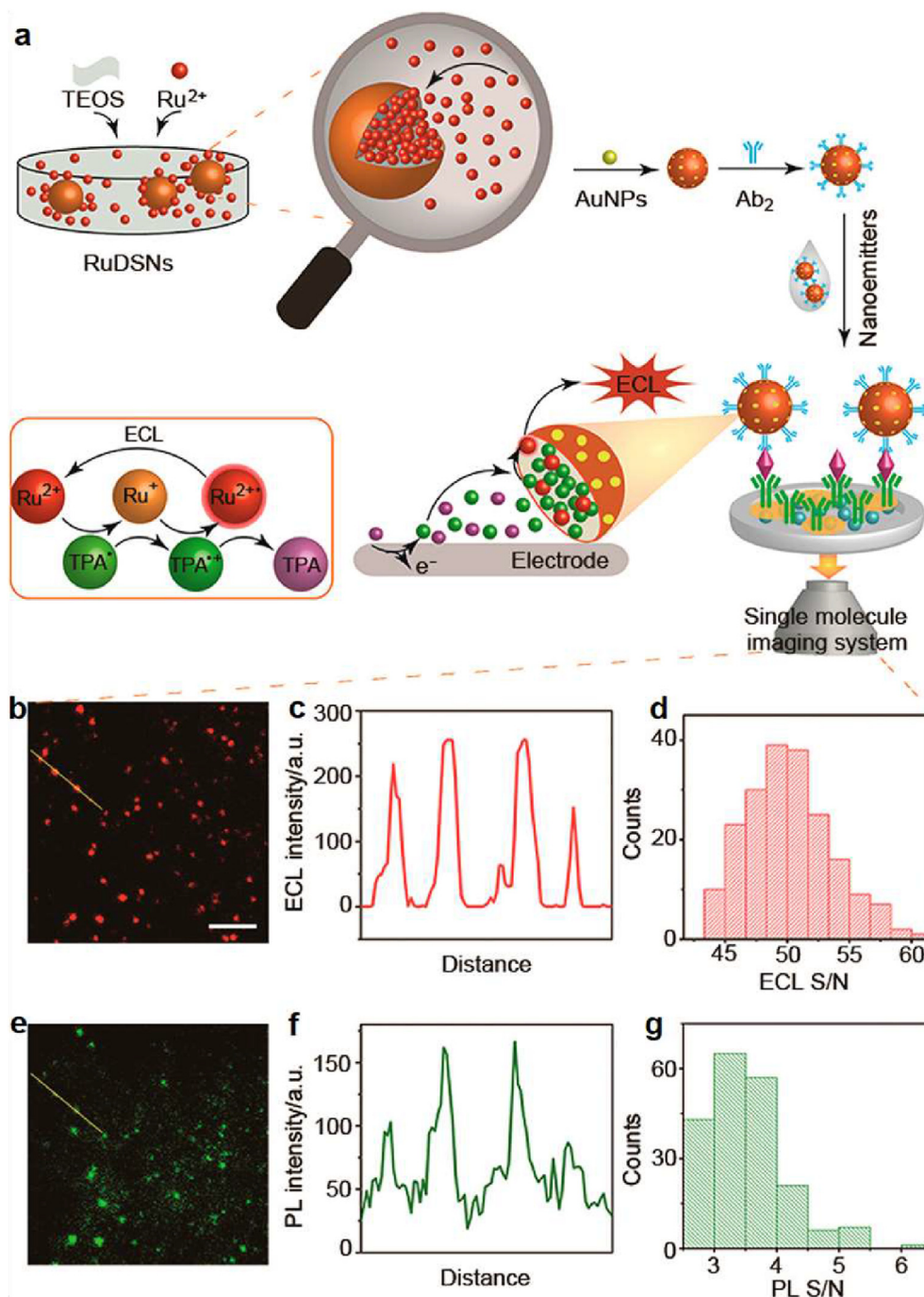


Fig. 8. Schematic illustration of single-protein-molecule imaging by ECL, and ECL/PL images of the same region of interest with individual nano-emitters immobilized on the ITO electrode [99]. Reproduced from Ref. [99] with permission from the American Chemical Society.

Following a similar principle, more efficient ECL imaging methods can be realized by combining ECL and nanomaterials, such as Ru(bpy)₃²⁺-doped silica/Au nanoparticles, quantum dots, and carbon dots [98]. Liu et al. imaged a single biomolecule on an electrode surface and cellular membrane proteins (Fig. 8) [99]. Ru(bpy)₃²⁺-doped silica/Au nanoparticles (RuDSNs/AuNPs) served as nano-emitters attached to the antibody to label the cellular membrane. This approach led to enhancement of the ECL signal due to the local surface confinement effect. Additionally, the absence of photobleaching and background signal provided a 6.5-fold increase in the S/N ratio compared to PL, allowing the study of the membrane's low protein content. Furthermore, label-free imaging of antigens on the cellular membrane was achieved using the luminol/H₂O₂ co-reactant system's dependence on the voltage drop (V_{dl}) [100]. Specifically, if the non-conductive object is attached to the cellular membrane, capacitance in the binding region will decrease, leading to an elevated V_{dl} and consequently to a brighter luminescence in this region. This approach has been studied by binding carcinoembryonic antigens to the cellular surface and applying a square wave voltage, thus proving that sensitive and selective imaging of single objects on the cellular surface is possible non-invasively and without cell modification.

Recently, two reports yielded important information on the fundamental properties of ECL microscopy of cells, which potentially point to the development of new ECL methods. Both studies are associated with signal attenuation and rely on the well-investigated and previously described system consisting of Ru(bpy)₃²⁺ derivative labeled cells attached on a GCE surface and a freely diffusing TPA co-reactant. An investigation of the influence of photobleaching on ECL showed a direct correlation between illumination time and PL and ECL signal attenuation, proving that photo- and electro-excitation both generate the same excited state [101]. Consecutive anodic pulses also led to ECL fading, with the first ECL signal being five times more intense than the second and twelve times more than the fifth [102]. A cathodic treatment was proposed and resulted in the retention of the ECL intensity, and even its slight elevation during the second and third pulses after cathodic regeneration. The obtained results suggest that the TPA and/or the electrogenerated TPA radicals adsorbed on the electrode surface and the cathodic treatment renewed it, or that regeneration influenced the hydrophobicity of the electrode and, accordingly, the ECL signal generation.

The formation of cell–cell junctions and cell–matrix adhesions with the extracellular matrix play essential roles in cell migration, wound healing processes, tissue organization, tumorigenesis, and cancer morphogenesis; cell–cell junctions incorporate cells into three-dimensional tissues and regulate various biological processes. For that reason, understanding the distribution, strength, and dynamic variation of these regions of attachment can provide valuable information for medicine and biology. Ding et al. reported the use of ECL for label-free studying of cell–matrix adhesions and the migration of living cells using an ITO electrode modified with a silica nanochannel membrane (Fig. 9) [103]. The membrane, being non-conductive and biocompatible, improved cell attachment, reduced cell perturbation, and introduced a space between the electrode and the cell, allowing better contrast between bound and non-bound cell regions, while its negatively charged vertical nanochannels enhanced the ECL signal. In the reported configuration, ECL originated from electro-oxidation of the luminophore and co-reactant freely diffusing in the solution. The adhesion sites blocked the luminophore and co-reactant from diffusing to the electrode surface and oxidizing, resulting in dark regions (shadows) in the ECL image. Observations of a single cell provided data on the adhesion strength by incubating the cell with trypsin and following the decrease in shadow area relative to the incubation time. Since weak adhesions were digested by trypsin more rapidly than strong ones, adhesion and digestion rates within a single cell could be spatially distinguished. Similarly, by performing a wound-healing assay, dynamic ECL was employed to follow the cell–matrix adhesions of multiple cells to determine their orientations

and movement; this involved surface confinement of ECL using a high concentration of co-reactant [103].

By decreasing co-reactant and increasing luminophore concentrations, the ECL region can be expanded, enabling the study of cell–cell junctions. The influence of luminophore concentration on the modulation of the ECL layer thickness was first confirmed on an inert photoresist spot and subsequently applied to sequential imaging of cell–cell junctions and cell–matrix adhesion [104]. In a similar strategy, an imaged object hindered the local diffusion of ECL reagents, generating a negative imprint that was used to visualize single functional mitochondria [105].

Gao et al. used ECL to quantify MCF-7 cells captured on an aminophenol-functionalized GCE with a low LOD of 29 cells/mL, and to evaluate the influence of H₂O₂ and electrical stimulation on their morphology [106]. They proved that prolonged H₂O₂ stimulation weakens adhesion, which leads to cell shrinkage and rounding, causing cells to disconnect from those surrounding them and detach from the surface. On the other hand, electrical stimulation (0.8 V) has the opposite impact. The cells tend to aggregate, which is evident from an increase in the cell boundary and a decrease in the junction distance. ECL as an in situ method bypasses the labeling step and allows both single-cell analysis and quantitative determination [106].

The abovementioned approaches to ECL imaging, although introducing innovations for analyzing single objects, applying in diagnostics, and understanding the heterogeneity of cell properties, have certain drawbacks. Firstly, due to the short lifetimes of the co-reactant radical species, ECL is confined to the electrode surface, and it is impossible to image the whole cell without permeabilization. Secondly, the most commonly used alkyl amine co-reactants are relatively toxic and corrosive. Attempts to overcome these problems have focused on utilizing biomolecules as co-reactant species. In this strategy, Ru(bpy)₃²⁺ is oxidized at the electrode and reacts with intracellular biomolecules acting as co-reactants to achieve imaging of intracellular structures, dynamic transport through the membrane, and real-time tracking of the influence of environmental factors on biomolecules. Whether a molecule can function as a co-reactant is determined by its first ionization potential, which is low for the guanine moieties of nucleic acids and the imidazole in histidine. However, since the luminophore cannot pass through the cellular membrane, permeabilization or electroporation is required, so the method involves a level of destruction. Nonetheless, it has zero toxicity, does not require cell labeling, and can image all intracellular structures, because the ECL layer is very thick due to the long lifetime of the ruthenium bipyridyl species [107]. The other possible approach relies on new co-reactant material synthesis. Guanine-rich single-stranded DNA (G-ssDNA) has higher ECL efficiency than DNA because of the former's lower steric hindrance. Incorporating G-ssDNA

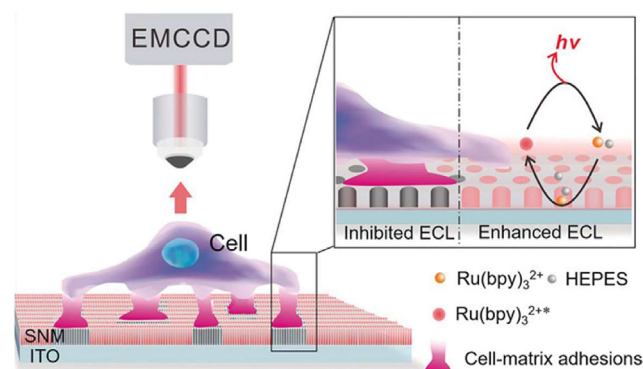


Fig. 9. Using electrochemiluminescence microscopy using silica nanochannel membrane (SNM), enabling ECL reactants confinement for imaging cell–matrix adhesion and the collective migration of living cells [103]. Reproduced from Ref. [103] with permission from John Wiley and Sons.

into a high-index faceted gold nanoflower (Hi-AuNF), which had a high specific surface area and outstanding catalytic properties, leads to remarkable ECL signal enhancement. Here, Hi-AuNF serves as both an ECL enhancer and a carrier for G-ssDNA to enable the specific identification of membrane proteins on cancer cells [108]. Tertiary amine conjugated polymer dots (TEA-Pdots) have been developed as an in situ co-reactant-embedded ECL system to image membrane proteins. The reported co-reactant-embedded mechanism — which introduced polymer conductivity, hybridization-induced catalytic properties, biocompatibility, and non-toxicity — provided several advantageous features, including a low working potential (1.2 V), the ability to image

non-permeabilized cells, and increased ECL efficiency compared to a traditional ECL system [109].

Feng et al. reported a combined optical imaging and electrochemical recording system for monitoring single molecule $\text{Ru}(\text{bpy})_3^{2+}$ -based ECL reactions in aqueous solutions, achieving a resolution down to 22 nm [86]. This was enabled by a correlative super-resolution imaging and electrochemical recording system (Fig. 10). This single-photon microscopy approach allowed the observation of individual chemical events in solution. In fact, the authors demonstrated the imaging of the spatial distribution of single photons resulting from individual ECL-based reactions. They then extended their approach to image cells. Recent

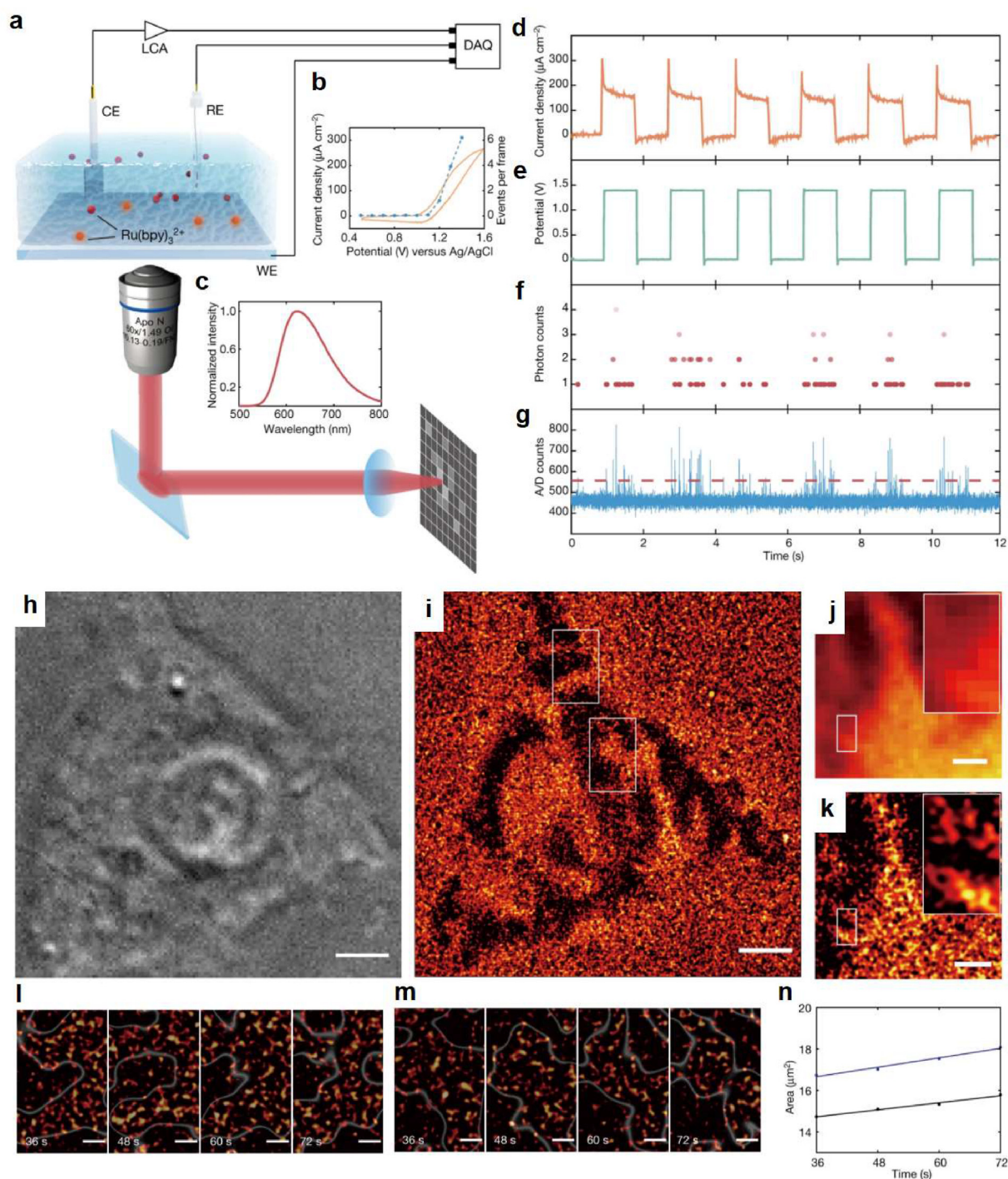


Fig. 10. Single-molecule ECL imaging device (a), observation of random reactions (d–f), and single-molecule ECL imaging of live cells (h–n) [86]. Reproduced from Ref. [86] with permission from Nature Portfolio.

advances in ECL show that it is transforming from a sensitive analytical technique to a powerful imaging method, enabling single-molecule resolution. Due to its electrochemical step, ECL should be considered a dynamic technique with high spatiotemporal resolution that can give real-time information about the processes happening in cells and at the cell–matrix interface, rather than just a microscopic imaging method.

Chen et al. performed imaging analysis of dynamic cellular processes based on photodynamic therapy (PDT). In PDT, Ru(bpy)₃²⁺/TPA is not only the optical component of ECL imaging but also the light source for ROS produced by the photosensitizer. After receiving the energy transfer, the photosensitizer Ce6 sensitized the surrounding O₂ to ROS. Using an ECL microscope, it was possible to observe cell deformation, cell mechanism adhesion changes, and cell membrane permeability changes in the ECL–PDT process and to achieve real-time imaging of cells [110].

5. Conclusion and future perspective

ECL is a promising dual electrochemical/optical technique for generating light emission events with close to zero background light noise. Over the past few years, this has enabled ECL to shift from (bio) chemical assay detection to strategies for imaging objects and (bio) chemical reactions. ECL-based imaging strategies have been implemented at the nanometer or micrometer scale and are widely used to visualize single cells, microspheres, and nanoobjects such as nanoparticles or nanowires with spatial resolutions approaching those of standard optical microscopies. Recent progress has pushed the spatial resolution and sensitivity limits of ECL microscopies by demonstrating methods for imaging objects at the ultimate limit of a single molecule, a single photon, or even a single chemical reaction. Strategies are also currently being proposed to use ECL readouts as a means to characterize electrocatalytic reactions. Although this has so far been restricted to reaction schemes producing light emissions (i.e., involving the fluorophore or one of the electrogenerated intermediates issuing from the co-reactant), combining this strategy with ECL imaging should enable the screening of different nanocatalysts (e.g., for the ORR) [111–113].

Overall, these recent approaches will considerably widen the possibilities for using ECL imaging to more comprehensively explore the reaction modes of nanocatalysts. One could foresee further progress along this new avenue, taking inspiration from single-molecule fluorescence microscopy, for example, to broaden the range of electrocatalytic reactions of interest [114–117]. Alternatively, one could combine the strategies developed in life sciences using (bio)chemiluminescence microscopies [118].

ECL microscopy has also made some important progress in analytical chemistry for the life sciences by enabling the imaging of single cells and protein distributions. At present, ECL microscopic imaging research urgently needs to develop new ECL systems, design new and efficient ECL probes, and improve luminescence efficiency. In the future, the development of a highly sensitive, high-intensity ECL single-molecule imaging system could be a major milestone for early disease detection, diagnosis, and treatment.

Declaration of competing interest

The authors declare that they have no known competing financial interests or personal relationships that could have appeared to influence the work reported in this paper.

Acknowledgments

The authors thank National Natural Science Foundation of China (Nos. 21874126 and 22174136), the CAS President's International Fellowship Initiative (PIFI), the Agence Nationale de la Recherche (ELISE – ANR-21-CE42), the Translation of Combination Research of First Hospital of Jilin University and Changchun Institute of Applied

Chemistry, Chinese Academy of Sciences, CAS-VPST Silk Road Science Fund 2021 (GJHZ202125 and INSF 99008701) for financial support.

References

- W.J. Miao, Electrogenerated chemiluminescence and its biorelated applications, *Chem. Rev.* 108 (2008) 2506–2553.
- J.T. Cao, Y.L. Wang, J.J. Zhang, Y.X. Dong, F.R. Liu, S.W. Ren, Y.M. Liu, Immuno-electrochemiluminescent imaging of a single cell based on functional nanopores of heterogeneous Ru(bpy)₃²⁺@SiO₂/Au nanoparticles, *Anal. Chem.* 90 (2018) 10334–10339.
- W.L. Gu, H.J. Wang, L. Jiao, Y. Wu, Y.X. Chen, L.Y. Hu, J.M. Gong, D. Du, C.Z. Zhu, Single-atom iron boosts electrochemiluminescence, *Angew. Chem. Int. Ed.* 59 (2020) 3534–3538.
- Z.G. Han, Z.F. Yang, H.S. Sun, Y.L. Xu, X.F. Ma, D.L. Shan, J. Chen, S.H. Huo, Z. Zhang, P.Y. Du, X.Q. Lu, Electrochemiluminescence platforms based on small water-insoluble organic molecules for ultrasensitive aqueous-phase detection, *Angew. Chem. Int. Ed.* 58 (2019) 5915–5919.
- Y.P. He, L.Q. Yang, F. Zhang, B. Zhang, G.Z. Zou, Tunable electron-injection channels of heterostructured ZnSe@CdTe nanocrystals for surface-chemistry-involved electrochemiluminescence, *J. Phys. Chem. Lett.* 9 (2018) 6089–6095.
- Irkham, A. Fiorani, G. Valenti, N. Kamoshida, F. Paolucci, Y. Einaga, Electrogenerated chemiluminescence by in situ production of coreactant hydrogen peroxide in carbonate aqueous solution at a boron-doped diamond electrode, *J. Am. Chem. Soc.* 142 (2020) 1518–1525.
- G. Pitingolo, P. Nizard, A. Riaud, V. Taly, Beyond the on/off chip trade-off: a reversibly sealed microfluidic platform for 3D tumor microtissue analysis, *Sens. Actuators B Chem.* 274 (2018) 393–401.
- E. Da-Silva, J. Baudart, L. Barthelmebs, Biosensing platforms for vibrio bacteria detection based on whole cell and nucleic acid analysis: a review, *Talanta* 190 (2018) 410–422.
- S. Carrara, F. Arcudi, M. Prato, L. De Cola, Amine-rich nitrogen-doped carbon nanodots as a platform for self-enhancing electrochemiluminescence, *Angew. Chem. Int. Ed.* 56 (2017) 4757–4761.
- Y. Cao, Z.Y. Zhang, L.L. Li, J.R. Zhang, J.J. Zhu, An improved strategy for high-quality cesium bismuth bromine perovskite quantum dots with remarkable electrochemiluminescence activities, *Anal. Chem.* 91 (2019) 8607–8614.
- Z.Y. Cao, Y.F. Shu, H.Y. Qin, B. Su, X.G. Peng, Quantum dots with highly efficient, stable, and multicolor electrochemiluminescence, *ACS Cent. Sci.* 6 (2020) 1129–1137.
- M.H. Wang, J.J. Liu, X. Liang, R.Y. Gao, Y.M. Zhou, X. Nie, Y. Shao, Y. Guan, L.M. Fu, J.P. Zhang, Y.H. Shao, Electrochemiluminescence based on a dual carbon ultramicroelectrode with confined steady-state annihilation, *Anal. Chem.* 93 (2021) 4528–4535.
- F. Wang, J. Lin, S.S. Yu, X.Q. Cui, A. Ali, T. Wu, Y. Liu, Anti-site defects-assisted enhancement of electrogenerated chemiluminescence from in situ Mn²⁺-doped supertetrahedral chalcogenide nanoclusters, *ACS Appl. Mater. Interfaces* 10 (2018) 38223–38229.
- A. Zanut, F. Palomba, M.R. Scota, S. Rebecani, M. Marcaccio, D. Genovese, E. Rampazzo, G. Valenti, F. Paolucci, L. Prodi, Dye-doped silica nanoparticles for enhanced ECL-based immunoassay analytical performance, *Angew. Chem. Int. Ed.* 59 (2020) 21858–21863.
- Y.M. Zhang, F. Wang, H.X. Zhang, H.Y. Wang, Y. Liu, Multivalency interface and g-C₃N₄ coated liquid metal nanoprobe signal amplification for sensitive electrogenerated chemiluminescence detection of exosomes and their surface proteins, *Anal. Chem.* 91 (2019) 12100–12107.
- M.J. Zhu, J.B. Pan, Z.Q. Wu, X.Y. Gao, W. Zhao, X.H. Xia, J.J. Xu, H.Y. Chen, Electrogenerated chemiluminescence imaging of electrocatalysis at a single Au-pyrene nanoparticle, *Angew. Chem. Int. Ed.* 57 (2018) 4010–4014.
- X. Tan, B. Zhang, G.Z. Zou, Electrochemistry and electrochemiluminescence of organometal halide perovskite nanocrystals in aqueous medium, *J. Am. Chem. Soc.* 139 (2017) 8772–8776.
- F. Zinna, S. Voci, L. Arrico, E. Brun, A. Homberg, L. Bouffier, T. Funaioli, J. Lacour, N. Sojic, L. Di Bari, Circularly-polarized electrochemiluminescence from a chiral bispyrene organic macrocycle, *Angew. Chem. Int. Ed.* 58 (2019) 6952–6956.
- L. Gamiz-Gracia, A.M. Garcia-Campana, J.F. Huertas-Perez, F.J. Lara, Chemiluminescence detection in liquid chromatography: applications to clinical, pharmaceutical, environmental and food analysis—a review, *Anal. Chim. Acta* 640 (2009) 7–28.
- Y. Sun, Y.M. Zhang, H.X. Zhang, M.L. Liu, Y. Liu, Integrating highly efficient recognition and signal transition of g-C₃N₄ embellished Ti₃C₂ mxene hybrid nanosheets for electrogenerated chemiluminescence analysis of protein kinase activity, *Anal. Chem.* 92 (2020) 10668–10676.
- G. Valenti, E. Rampazzo, S. Bonacchi, L. Petrizza, M. Marcaccio, M. Montalti, L. Prodi, F. Paolucci, Variable doping induces mechanism swapping in electrogenerated chemiluminescence of Ru(bpy)₃²⁺ core-shell silica nanoparticles, *J. Am. Chem. Soc.* 138 (2016) 15935–15942.
- Z.Y. Cao, B. Su, Light enhanced electrochemistry and electrochemiluminescence of luminol at glassy carbon electrodes, *Electrochem. Commun.* 98 (2019) 47–52.
- X.K. Kong, C. Wang, L. Pu, P.P. Gai, F. Li, Self-photocatalysis boosted electrochemiluminescence signal amplification via in situ generation of the coreactant, *Anal. Chem.* 93 (2021) 12441–12446.
- M.M. Chen, C.H. Xu, W. Zhao, H.Y. Chen, J.J. Xu, Observing the structure-dependent electrocatalytic activity of bimetallic Pd-Au nanorods at the single-particle level, *Chem. Commun.* 56 (2020) 3413–3416.

- [25] C. Ma, W.W. Wu, L.L. Li, S.J. Wu, J.R. Zhang, Z.X. Chen, J.J. Zhu, Dynamically imaging collision electrochemistry of single electrochemiluminescence nanoemitters, *Chem. Sci.* 9 (2018) 6167–6175.
- [26] M. Mayer, S. Takegami, M. Neumeier, S. Rink, A. Jacobi von Wangelin, S. Schulte, M. Vollmer, A.G. Griesbeck, A. Duerkop, A.J. Baeumner, Electrochemiluminescence bioassays with a water-soluble luminol derivative can outperform fluorescence assays, *Angew. Chem. Int. Ed.* 57 (2018) 408–411.
- [27] W.L. Guo, H. Ding, C.Y. Gu, Y.H. Liu, X.C. Jiang, B. Su, Y.H. Shao, Potential-resolved multicolor electrochemiluminescence for multiplex immunoassay in a single sample, *J. Am. Chem. Soc.* 140 (2018) 15904–15915.
- [28] S. Chen, H. Ma, J.W. Padelford, W. Qinchen, W. Yu, S. Wang, Near infrared electrochemiluminescence of rod-shape 25-atom AuAg nanoclusters that is hundreds-fold stronger than that of Ru(bpy)₃²⁺ standard, *J. Am. Chem. Soc.* 141 (2019) 9603–9609.
- [29] Y.P. He, S.F. Hou, L.Q. Yang, F. Zhang, G.Z. Zou, Adjustable Electrochemiluminescence from highly passivated CdTe/CdS nanocrystals by simple surface decoration with counterions, *Chem. Eur. J.* 24 (2018) 9592–9597.
- [30] Y. Chen, S.W. Zhou, L.L. Li, J.J. Zhu, Nanomaterials-based sensitive electrochemiluminescence biosensing, *Nano Today* 12 (2017) 98–115.
- [31] J.W. Sun, H. Sun, Z.Q. Liang, Nanomaterials in electrochemiluminescence sensors, *ChemElectroChem* 4 (2017) 1651–1662.
- [32] M.M. Chen, W. Zhao, M.J. Zhu, X.L. Li, C.H. Xu, H.Y. Chen, J.J. Xu, Spatiotemporal imaging of electrocatalytic activity on single 2D gold nanoplates via electrogenerated chemiluminescence microscopy, *Chem. Sci.* 10 (2019) 4141–4147.
- [33] Z.H. Liang, Q. Zhang, Y.X. Nie, X. Zhang, Q. Ma, Polarized-electrochemiluminescence biosensor based on surface plasmon coupling strategy and fluorine-doped BN quantum dots, *Anal. Chem.* 92 (2020) 9223–9229.
- [34] X.W. Zheng, Z.H. Guo, Z.J. Zhang, Flow-injection electrogenerated chemiluminescence determination of isoniazid using luminol, *Anal. Sci.* 17 (2001) 1095–1099.
- [35] C. Ma, H.F. Wei, M.X. Wang, S.J. Wu, Y.C. Chang, J.R. Zhang, L.P. Jiang, W.L. Zhu, Z.X. Chen, Y.H. Lin, Hydrogen evolution reaction monitored by electrochemiluminescence blinking at single-nanoparticle level, *Nano Lett.* 20 (2020) 5008–5016.
- [36] A.W. Knight, A review of recent trends in analytical applications of electrogenerated chemiluminescence, *TrAC-Trends Anal. Chem.* 18 (1999) 47–62.
- [37] S. Manago, G. Zito, A.C. De Luca, Raman microscopy based sensing of leukemia cells: a review, *Opt. Laser Technol.* 108 (2018) 7–16.
- [38] Q.F. Zhai, J. Li, E.K. Wang, Recent advances based on nanomaterials as electrochemiluminescence probes for the fabrication of sensors, *ChemElectroChem* 4 (2017) 1639–1650.
- [39] F. Wang, J. Lin, H.Y. Wang, S.S. Yu, X.Q. Cui, A. Ali, T. Wu, Y. Liu, Precise mono-Cu⁺ ion doping enhanced electrogenerated chemiluminescence from Cd-In-S supertetrahedral chalcogenide nanoclusters for dopamine detection, *Nanoscale* 10 (2018) 15932–15937.
- [40] K.N. Swanick, S. Ladouceur, E. Zysman-Colman, Z.F. Ding, Bright electrochemiluminescence of iridium(III) complexes, *Chem. Commun.* 48 (2012) 3179–3181.
- [41] G.Q. Pu, Z.F. Yang, Y.L. Wu, Z. Wang, Y. Deng, Y.J. Gao, Z. Zhang, X.Q. Lu, Investigation into the oxygen-involved electrochemiluminescence of porphyrins and its regulation by peripheral substituents/central metals, *Anal. Chem.* 91 (2019) 2319–2328.
- [42] W.J. Miao, J.P. Choi, A.J. Bard, Electrogenerated chemiluminescence 69: the tris(2,2'-bipyridine)ruthenium(II) (Ru(bpy)₃²⁺)/tri-n-propylamine (TPra) system revisited - a new route involving TPra(center dot+) cation radicals, *J. Am. Chem. Soc.* 124 (2002) 14478–14485.
- [43] Rebecani, A. Zanut, C.I. Santo, G. Valenti, F. Paolucci, A guide inside electrochemiluminescent microscopy mechanisms for analytical performance improvement, *Anal. Chem.* 94 (2022) 336–348.
- [44] A. Zanut, A. Fiorani, S. Canola, T. Saito, N. Ziebart, S. Rapino, S. Rebecani, A. Barbon, T. Irie, H.P. Josel, F. Negri, M. Marcaccio, M. Windfuhr, K. Imai, G. Valenti, F. Paolucci, Insights into the mechanism of coreactant electrochemiluminescence facilitating enhanced bioanalytical performance, *Nat. Commun.* 11 (2020) 1–9.
- [45] Y.X. Wu, Z.G. Han, L.P. Wei, H.S. Sun, T.Y. Wang, J. Chen, R.Z. Zhang, X.Q. Lu, Depolymerization-induced electrochemiluminescence of insoluble porphyrin in aqueous phase, *Anal. Chem.* 92 (2020) 5464–5472.
- [46] L.Q. Yang, B. Zhang, L. Fu, K.N. Fu, G.Z. Zou, Efficient and monochromatic electrochemiluminescence of aqueous-soluble Au nanoclusters via host-guest recognition, *Angew. Chem. Int. Ed.* 58 (2019) 6901–6905.
- [47] C. Amatore, C. Pebay, L. Servant, N. Sojic, S. Szunerits, L. Thouin, Mapping electrochemiluminescence as generated at double-band microelectrodes by confocal microscopy under steady state, *ChemPhysChem* 7 (2006) 1322–1327.
- [48] S. Szunerits, P. Garrigue, J.L. Bruneel, L. Servant, N. Sojic, Fabrication of a sub-micrometer electrode array: electrochemical characterization and mapping of an electroactive species by confocal Raman microspectroscopy, *Electroanalysis* 15 (2003) 548–555.
- [49] Z.J. Lin, X.M. Chen, T.T. Jia, X.D. Wang, Z.X. Xie, M. Oyama, X. Chen, Fabrication of a colorimetric electrochemiluminescence sensor, *Anal. Chem.* 81 (2009) 830–833.
- [50] F. Deiss, C.N. LaFratta, M. Symer, T.M. Blicharz, N. Sojic, D.R. Walt, Multiplexed sandwich immunoassays using electrochemiluminescence imaging resolved at the single bead level, *J. Am. Chem. Soc.* 131 (2009) 6088–6089.
- [51] Z.Y. Zhou, L.R. Xu, S.Z. Wu, B. Su, A novel biosensor array with a wheel-like pattern for glucose, lactate and choline based on electrochemiluminescence imaging, *Analyst* 139 (2014) 4934–4939.
- [52] Visual electrochemiluminescence detection of telomerase activity based on multifunctional Au nanoparticles modified with G-quadruplex deoxyribozyme and luminol, *Chem. Commun.* 50 (2014) 12575–12577.
- [53] A. Chovin, P. Garrigue, N. Sojic, Electrochemiluminescent detection of hydrogen peroxide with an imaging sensor array, *Electrochim. Acta* 49 (2004) 3751–3757.
- [54] L. Bouffier, D. Manojlovic, A. Kuhn, N. Sojic, Advances in bipolar electrochemiluminescence for the detection of biorelevant molecular targets, *Curr. Opin. Electrochem.* 16 (2019) 28–34.
- [55] X. Zhang, S.N. Ding, Graphite paper-based bipolar electrode electrochemiluminescence sensing platform, *Biosens. Bioelectron.* 94 (2017) 47–55.
- [56] L. Bouffier, S. Arbault, A. Kuhn, N. Sojic, Generation of electrochemiluminescence at bipolar electrodes: concepts and applications, *Anal. Bioanal. Chem.* 408 (2016) 7003–7011.
- [57] H.R. Zhang, Y.Z. Wang, W. Zhao, J.J. Xu, H.Y. Chen, Visual color-switch electrochemiluminescence biosensing of cancer cell based on multichannel bipolar electrode chip, *Anal. Chem.* 88 (2016) 2884–2890.
- [58] S. Baek, S.R. Kwon, S.Y. Yeon, S.H. Yoon, C.M. Kang, S.H. Han, D. Lee, T.D. Chung, Miniaturized reverse electroanalysis-powered biosensor using electrochemiluminescence on bipolar electrode, *Anal. Chem.* 90 (2018) 4749–4755.
- [59] R. Liu, C.S. Zhang, M. Liu, Open bipolar electrode-electrochemiluminescence imaging sensing using paper-based microfluidics, *Sens. Actuators B Chem.* 216 (2015) 255–262.
- [60] S.F. Douman, D. Collins, L.R. Cumba, S. Beirne, G.G. Wallace, Z.L. Yue, E.I. Iwuoha, F. Melinato, Y. Pellegrin, R.J. Forster, Wireless electrochemiluminescence at functionalised gold microparticles using 3D titanium electrode arrays, *Chem. Commun.* 57 (2021) 4642–4645.
- [61] X.G. Ma, W.Y. Gao, F.X. Du, F. Yuan, J. Yu, Y.R. Guan, N.O. Sojic, G.B. Xu, Rational design of electrochemiluminescent devices, *Accounts Chem. Res.* 54 (2021) 2936–2945.
- [62] J. Totorigaena-Gorrino, M. Dei, A.F. Alba, N. Perinka, L.R. Rubio, J.L. Vilas-Vilela, F.J. del Campo, Toward next-generation mobile diagnostics: near-field electrocommunication-powered electrochemiluminescent detection, *ACS Sens.* 7 (2022) 1544–1554.
- [63] M.S. Wu, H.W. Shi, L.J. He, J.J. Xu, H.Y. Chen, Microchip device with 64-site electrode array for multiplexed immunoassay of cell surface antigens based on electrochemiluminescence resonance energy transfer, *Anal. Chem.* 84 (2012) 4207–4213.
- [64] C.A. Marquette, L.J. Blum, Self-containing reactant biochips for the electrochemiluminescent determination of glucose, lactate and choline, *Sens. Actuators B Chem.* 90 (2003) 112–117.
- [65] N.P. Sardesai, J.C. Barron, J.F. Rusling, Carbon nanotube microwell array for sensitive electrochemiluminescent detection of cancer biomarker proteins, *Anal. Chem.* 83 (2011) 6698–6703.
- [66] M.S. Wu, Z. Liu, H.W. Shi, H.Y. Chen, J.J. Xu, Visual electrochemiluminescence detection of cancer biomarkers on a closed bipolar electrode array chip, *Anal. Chem.* 87 (2015) 530–537.
- [67] L.M. Qi, Y. Xia, W.J. Qi, W.Y. Gao, F.X. Wu, G.B. Xu, Increasing electrochemiluminescence intensity of a wireless electrode array chip by thousands of times using a diode for sensitive visual detection by a digital camera, *Anal. Chem.* 88 (2016) 1123–1127.
- [68] T. Iwama, Y.Y. Guo, S. Handa, K.Y. Inoue, T. Yoshinobu, F. Sorin, H. Shiku, Thermally-drawn multi-electrode fibres for bipolar electrochemistry and magnified electrochemical imaging, *Adv. Mater. Technol. US* 7 (2022) 2101066.
- [69] M. Sentic, F. Virgilio, A. Zanut, D. Manojlovic, S. Arbault, M. Tormen, N. Sojic, P. Ugo, Microscopic imaging and tuning of electrogenerated chemiluminescence with boron-doped diamond nanoelectrode arrays, *Anal. Bioanal. Chem.* 408 (2016) 7085–7094.
- [70] F.X. Du, Z.Y. Dong, Y.R. Guan, A.M. Zeid, D. Ma, J.C. Feng, D. Yang, G.B. Xu, Single-electrode electrochemical system for the visual and high-throughput electrochemiluminescence immunoassay, *Anal. Chem.* 94 (2022) 2189–2194.
- [71] F.T. Patrice, K.P. Qiu, Y.L. Ying, Y.T. Long, Single nanoparticle electrochemistry, *Annu. Rev. Anal. Chem.* 12 (2019) 347–370.
- [72] T. Albrecht, S. Horswell, L.K. Allerston, N.V. Rees, P. Rodriguez, Electrochemical processes at the nanoscale, *Curr. Opin. Electrochem.* 7 (2018) 138–145.
- [73] C.L. Bentley, J. Edmondson, G.N. Meloni, D. Perry, V. Shkirskiy, P.R. Unwin, Nanoscale electrochemical mapping, *Anal. Chem.* 91 (2019) 84–108.
- [74] J.F. Lemineur, H. Wang, W. Wang, F. Kanoufi, Emerging optical microscopy techniques for electrochemistry, *Annu. Rev. Anal. Chem.* 15 (2022) 57–82.
- [75] F. Kanoufi, *Electrochemistry and optical microscopy*, in: *Encyclopedia of Electrochemistry* 22, 2021, <https://doi.org/10.1002/9783527610426.bard030108>.
- [76] F.R.F. Fan, A.J. Bard, Observing single nanoparticle collisions by electrogenerated chemiluminescence amplification, *Nano Lett.* 8 (2008) 1746–1749.
- [77] F.R.F. Fan, S. Park, Y.W. Zhu, R.S. Ruoff, A. J. Bard, Electrogenerated chemiluminescence of partially oxidized highly oriented pyrolytic graphite surfaces and of graphene oxide nanoparticles, *J. Am. Chem. Soc.* 131 (2009) 937–939.
- [78] S.L. Pan, J. Liu, C.M. Hill, Observation of local redox events at individual Au nanoparticles using electrogenerated chemiluminescence microscopy, *J. Phys. Chem. C* 119 (2015) 27095–27103.

- [79] V. Brasiliense, A.N. Patel, A. Martinez-Marrades, J. Shi, Y. Chen, C. Combellas, G. Tessier, F. Kanoufi, Correlated electrochemical and optical detection reveals the chemical reactivity of individual silver nanoparticles, *J. Am. Chem. Soc.* 138 (2016) 3478–3483.
- [80] R. Hao, Y.S. Fan, B. Zhang, Imaging dynamic collision and oxidation of single silver nanoparticles at the electrode/solution interface, *J. Am. Chem. Soc.* 139 (2017) 12274–12282.
- [81] F. Ben Trad, V. Wiczny, J. Delacotte, M. Morel, M. Guille-Collignon, S. Arbault, F. Lemaître, N. Sojic, E. Labbe, O. Buriez, Dynamic electrochemiluminescence imaging of single giant liposome opening at polarized electrodes, *Anal. Chem.* 94 (2022) 1686–1696.
- [82] Y. Fan, T.J. Anderson, B. Zhang, Single-molecule electrochemistry: from redox cycling to single redox events, *Curr. Opin. Electrochem.* 7 (2018) 81–86.
- [83] W. Wang, Imaging the chemical activity of single nanoparticles with optical microscopy, *Chem. Soc. Rev.* 47 (2018) 2485–2508.
- [84] Y. Chen, D.B. Zhao, J.J. Fu, X.D. Gou, D.C. Jiang, H. Dong, J.J. Zhu, In situ imaging facet-induced spatial heterogeneity of electrocatalytic reaction activity at the subparticle level via electrochemiluminescence microscopy, *Anal. Chem.* 91 (2019) 6829–6835.
- [85] J.R. Dong, Y. Xu, Z.Q. Zhang, J.D. Feng, Operando imaging of chemical activity on gold plates with single-molecule electrochemiluminescence microscopy, *Angew. Chem. Int. Ed.* 22 (2022) e202200187.
- [86] J.R. Dong, Y.X. Lu, Y. Xu, F.F. Chen, J.M. Yang, Y. Chen, J.D. Feng, Direct imaging of single-molecule electrochemical reactions in solution, *Nature* 596 (2021) 244–249.
- [87] F. Kanoufi, N. Sojic, A microscopy technique that images single reaction events in total darkness, *Nature* 596 (2021) 194–195.
- [88] H.Y. Xia, X.L. Zheng, J. Li, L.G. Wang, Y. Xue, C. Peng, Y.C. Han, Y. Wang, S.J. Guo, J. Wang, E. Wang, Identifying luminol electrochemiluminescence at the cathode via single-atom catalysts tuned oxygen reduction reaction, *J. Am. Chem. Soc.* 144 (2022) 7741–7749.
- [89] M.M. Chen, C.H. Xu, W. Zhao, H.Y. Chen, J.J. Xu, Super-resolution electrogenerated chemiluminescence microscopy for single-nanocatalyst imaging, *J. Am. Chem. Soc.* 143 (2021) 18511–18518.
- [90] L.R. Xu, Y. Li, S.Z. Wu, X.H. Liu, B. Su, Imaging latent fingerprints by electrochemiluminescence, *Angew. Chem. Int. Ed.* 51 (2012) 8068–8072.
- [91] L.R. Xu, Z.Y. Zhou, C.Z. Zhang, Y.Y. He, B. Su, Electrochemiluminescence imaging of latent fingerprints through the immunodetection of secretions in human perspiration, *Chem. Commun.* 50 (2014) 9097–9100.
- [92] S.J. Hu, Z.Y. Cao, L. Zhou, R.L. Ma, B. Su, Electrochemiluminescence imaging of latent fingerprints by electropolymerized luminol, *J. Electroanal. Chem.* 870 (2020) 114238.
- [93] X.X. Jian, J. Xu, Y.M. Wang, C.X. Zhao, Z.D. Gao, Y.Y. Song, Deployment of mil-88b(fe)/tio₂ nanotube-supported ti wires as reusable electrochemiluminescence microelectrodes for noninvasive sensing of H₂O₂ from single cancer cells, *Anal. Chem.* 93 (2021) 11312–11320.
- [94] N.N. Wang, H. Ao, W.C. Xiao, W.W. Chen, G.M. Li, J. Wu, H.X. Ju, Confined electrochemiluminescence imaging microarray for high-throughput biosensing of single cell-released dopamine, *Biosens. Bioelectron.* 201 (2022) 113959.
- [95] Y.L. Wang, R. Jin, N. Sojic, D.C. Jiang, H.Y. Chen, Intracellular wireless analysis of single cells by bipolar electrochemiluminescence confined in a nanopipette, *Angew. Chem. Int. Ed.* 59 (2020) 10416–10420.
- [96] G. Valentini, S. Scarabino, B. Goudeau, A. Lesch, M. Jovic, E. Villani, M. Sentic, S. Rapino, S. Arbault, F. Paolucci, N. Sojic, Single cell electrochemiluminescence imaging: from the proof-of-concept to disposable device-based analysis, *J. Am. Chem. Soc.* 139 (2017) 16830–16837.
- [97] S. Voci, B. Goudeau, G. Valentini, A. Lesch, M. Jovic, S. Rapino, F. Paolucci, S. Arbault, N. Sojic, Surface-confined electrochemiluminescence microscopy of cell membranes, *J. Am. Chem. Soc.* 140 (2018) 14753–14760.
- [98] F. Arcudi, L. Dordevic, S. Rebecani, M. Cacioppo, A. Zanut, G. Valentini, F. Paolucci, M. Prato, Lighting up the electrochemiluminescence of carbon dots through pre- and post-synthetic design, *Adv. Sci.* 8 (2021) 2100125.
- [99] Y.J. Liu, H.D. Zhang, B.X. Li, J.W. Liu, D.C. Jiang, B.H. Liu, N. Sojic, Single biomolecule imaging by electrochemiluminescence, *J. Am. Chem. Soc.* 143 (2021) 17910–17914.
- [100] J.J. Zhang, R. Jin, D.C. Jiang, H.Y. Chen, Electrochemiluminescence-based capacitance microscopy for label-free imaging of antigens on the cellular plasma membrane, *J. Am. Chem. Soc.* 141 (2019) 10294–10299.
- [101] D.N. Han, B. Goudeau, D. Manojlovic, D.C. Jiang, D.J. Fang, N. Sojic, Electrochemiluminescence loss in photobleaching, *Angew. Chem. Int. Ed.* 60 (2021) 7686–7690.
- [102] D.N. Han, B. Goudeau, D.C. Jiang, D.J. Fang, N. Sojic, Electrochemiluminescence microscopy of cells: essential role of surface regeneration, *Anal. Chem.* 93 (2021) 1652–1657.
- [103] H. Ding, W.L. Guo, B. Su, Imaging cell-matrix adhesions and collective migration of living cells by electrochemiluminescence microscopy, *Angew. Chem. Int. Ed.* 59 (2020) 449–456.
- [104] H. Ding, P. Zhou, W.X. Fu, L.R. Ding, W.L. Guo, B. Su, Spatially selective imaging of cell-matrix and cell-cell junctions by electrochemiluminescence, *Angew. Chem. Int. Ed.* 60 (2021) 11769–11773.
- [105] Y.M. Ma, C. Colin, J. Descamps, S. Arbault, N. Sojic, Shadow electrochemiluminescence microscopy of single mitochondria, *Angew. Chem. Int. Ed.* 60 (2021) 18742–18749.
- [106] H.F. Gao, W.J. Han, H.L. Qi, Q. Gao, C.X. Zhang, Electrochemiluminescence imaging for the morphological and quantitative analysis of living cells under external stimulation, *Anal. Chem.* 92 (2020) 8278–8284.
- [107] C. Ma, S.J. Wu, Y. Zhou, H.F. Wei, J.R. Zhang, Z.X. Chen, J.J. Zhu, Y.H. Lin, W.L. Zhu, Bio-coreactant-enhanced electrochemiluminescence microscopy of intracellular structure and transport, *Angew. Chem. Int. Ed.* 60 (2021) 4907–4914.
- [108] Y. Chen, X.D. Gou, C. Ma, D.C. Jiang, J.J. Zhu, A synergistic coreactant for single-cell electrochemiluminescence imaging: guanine-rich ssdna-loaded high-index faceted gold nanoflowers, *Anal. Chem.* 93 (2021) 7682–7689.
- [109] N.N. Wang, H. Gao, Y.Z. Li, G.M. Li, W.W. Chen, Z.C. Jin, J.P. Lei, Q. Wei, H.X. Ju, Dual intramolecular electron transfer for in situ coreactant-embedded electrochemiluminescence microimaging of membrane protein, *Angew. Chem. Int. Ed.* 60 (2021) 197–201.
- [110] M.M. Chen, C.H. Xu, W. Zhao, H.Y. Chen, J.J. Xu, Single cell imaging of electrochemiluminescence-driven photodynamic therapy, *Angew. Chem. Int. Ed.* 61 (2022) e202117401.
- [111] H. Yang, Y.F. Liu, X.L. Liu, X.K. Wang, H. Tian, G.I.N. Waterhouse, P.E. Kruger, S.G. Telfer, S.Q. Ma, Large-scale synthesis of N-doped carbon capsules supporting atomically dispersed iron for efficient oxygen reduction reaction electrocatalysis, *eScience 2* (2022) 227–234.
- [112] Y.J. Zhai, P. Han, Q.B. Yun, Y.Y. Ge, X. Zhang, Y. Chen, H. Zhang, Phase engineering of metal nanocatalysts for electrochemical CO₂ reduction, *eScience 2* (2022) 467–485.
- [113] Z.Y. Li, W.T. Wang, Q.Z. Qian, Y. Zhu, Y.F. Feng, Y.Y. Zhang, H.K. Zhang, M.Y. Cheng, G.Q. Zhang, Magic hybrid structure as multifunctional electrocatalyst surpassing benchmark Pt/C enables practical hydrazine fuel cell integrated with energy-saving H₂ production, *eScience 2* (2022) 416–427.
- [114] X.W. Mao, C.M. Liu, M. Hesari, N.M. Zou, P. Chen, Super-resolution imaging of non-fluorescent reactions via competition, *Nat. Chem.* 11 (2019) 687–694.
- [115] S.X. Li, J. Liang, P.P. Wei, Q. Liu, L.S. Xie, Y.L. Luo, X.P. Sun, ITO@TiO₂ nanoarray: an efficient and robust nitrite reduction reaction electrocatalyst toward NH₃ production under ambient conditions, *eScience 2* (2022) 382–388.
- [116] H. Shen, W.L. Xu, P. Chen, Single-molecule nanoscale electrocatalysis, *Phys. Chem. Chem. Phys.* 12 (2010) 6555–6563.
- [117] F.X. Meng, C.C. Dai, Z. Liu, S.Z. Luo, J.J. Ge, Y. Duan, G. Chen, C. Wei, R.R.X. Chen, J.R. Wang, D. Mandler, Z.C.J. Xu, Methanol electro-oxidation to formate on iron-substituted lanthanum cobaltite perovskite oxides, *eScience 2* (2022) 87–94.
- [118] Y.C. Yan, P.F. Shi, W.L. Song, S. Bi, Chemiluminescence and bioluminescence imaging for biosensing and therapy: in vitro and in vivo perspectives, *Theranostics* 9 (2019) 4047–4065.